Biological context modulates virus–host dynamics and diversification

Rodrigo Sanchez-Martinez[1], Esther Rubio-Portillo[1], Laura Medina-Ruiz[2], Jonás Sarasa[2], María Enciso[2], Fernando Santos[1,3]*, Josefa Antón[1,3,4]*

Affiliations

[1]Department of Physiology, Genetics and Microbiology, University of Alicante, San Vicent del Raspeig, Alicante, Spain

[2]IGLS, Alicante, Spain

[3]Institute of Health and Biomedical Research of Alicante (ISABIAL), Alicante, Spain

[4]Multidisciplinary Institute of Environmental Studies Ramon Margalef, Alicante, Spain

*Corresponding authors: fernando.santos@ua.es; anton@ua.es

ABSTRACT

Virus–bacterial interactions are fundamental to microbial ecology and evolution, but they have been studied mostly under simplified laboratory conditions. To better understand how ecological complexity shapes these dynamics, we examined the extreme halophilic bacterium *Salinibacter ruber* strain M1 and the EM1 virus in the presence of additional *Sal. ruber* strains and viruses. In the short term, the presence of other strains delayed lysis and reduced EM1 virus production, indicating that community composition directly affects viral replication. In the long term, both *Sal. ruber* M1 and the EM1 virus persisted across all experimental conditions, but their evolutionary responses differed. The EM1 virus showed an increased mutation rate, reduced infectivity against the native host, and expanded host range when other viruses were present, suggesting a previously unrecognized form of virus–virus interaction, in which coexisting viruses influence each other's evolutionary paths promoting viral diversification. In contrast, *Sal. ruber* M1 exhibited higher mutation rates evolving with other strains, indicating that in our system, intraspecific competition, rather than viral pressure, drives bacterial evolution. These findings demonstrate that incorporating biological complexity reveals distinct selective pressures acting on hosts and viruses, and is therefore essential for accurately predicting virus–host evolution in natural microbial ecosystems.

INTRODUCTION

Natural ecosystems are highly complex networks where multiple biotic and abiotic factors interact dynamically (Fuhrman et al., 2015; Levin, 1998). This complexity makes it challenging to predict ecological and evolutionary phenomena since experimental studies are generally conducted under simplified laboratory conditions which do not reflect natural dynamics (Calisi & Bentley, 2009; Chen et al., 2023; Roberts et al., 2015; Zimmer & Dorea, 2023). To advance our understanding of microbial processes and predict how microbial communities respond to environmental changes or selective pressures, it is crucial to design experiments that more faithfully simulate natural conditions, incorporating the diversity of species and interactions that characterize real ecosystems (Benton et al., 2007; Blazanin & Turner, 2021; Castledine & Buckling, 2024; Jessup et al., 2004).

Viruses act as major eco-evolutionary forces in microbial ecosystems. As the most abundant biological entities on Earth, they play a central role in regulating microbial communities through

diverse infection cycles that impact nutrient cycling, genetic diversity, and ecosystem structure (Fierer, 2017; Middelboe & Brussaard, 2017; Rohwer & Thurber, 2009). Virus–host interactions also drive microbial evolution, triggering adaptations that influence community composition and function. Despite their importance, many aspects of these interactions remain poorly understood, particularly under complex, natural conditions. Although numerous studies have explored virus–host interactions, most have relied on simplified experimental systems involving a single virus–host pair under controlled conditions. As a result, our understanding of how these interactions operate in more realistic settings remains limited. Investigating virus–host dynamics in environments that better mimic natural complexity is essential to fully grasp their ecological and evolutionary roles (Blazanin & Turner, 2021; Castledine & Buckling, 2024; Chevallereau et al., 2022; Koskella et al., 2022). While some recent efforts have incorporated greater biological complexity (Alseth et al., 2019, 2024; De Sordi et al., 2017; Gómez & Buckling, 2011, 2013; Middelboe et al., 2001; Mumford & Friman, 2017), such studies remain scarce. This persistent gap limits our ability to understand and predict how virus–host interactions shape microbial communities in natural ecosystems.

Hypersaline aquatic environments, which constitute approximately half of continental waters, harbor microbial communities that, at extreme salinities, are dominated by archaea (Burns et al., 2007; Shiklomanov, 1998; Ventosa, 2006). At these salinities, *Salinibacter ruber* emerges as the main bacterial species (Antón et al., 2002; Gomariz et al., 2015; Oren, 2011). Although *Sal. ruber* is as halophilic as the dominant archaea at close-to-saturation salinities, it is consistently less abundant, representing between 1% and 10% of total cells, indicating that it could be subjected to intense selective pressure (Mora-Ruiz et al., 2018; Ventosa et al., 2015). Cultivation and metagenomic studies reveal a high degree of intraspecific genomic diversity in *Sal. ruber*, including the coexistence of distinct phylogroups and adaptation to local microenvironments (Viver et al., 2015, 2023). These hypersaline habitats also harbor some of the highest recorded viral concentrations, with virus-like particles (VLP) reaching up to 10^{10} VLP/ml and virus-to-cell ratios ranging from 10 to 100 (Di Meglio et al., 2016; Santos et al., 2012). Given its environmental ubiquity, cultivability, and intraspecific variation, likely shaped in part by viral predation, *Sal. ruber* constitutes a valuable model for studying microbial ecology and virus–host interactions.

85 In this work, we have addressed how the ecology and evolution of a virus–host pair (i.e., *Sal. ruber*
86 strain M1 and the EM1 virus) are affected by the presence of additional *Sal. ruber* strains and their
87 viruses. Through experiments in which biological complexity is increased, we have demonstrated
88 that: (i) the presence of other strains and viruses delays lysis and reduces EM1 virion production;
89 and that (ii) the biological context influences the long-term evolution of the virus–host pair and
90 promotes changes in viral infectivity and host range, driven by a high mutation rate under more
91 complex contexts. These findings highlight the importance of considering biological complexity
92 in studies of virus–host interactions. Our work not only contributes to a better understanding of
93 these dynamics in natural systems but also suggests this complexity to be considered in practical
94 applications such as phage therapy and microbial community engineering.

95

96 **RESULTS AND DISCUSSION**

97 Five experiments were conducted in parallel to evaluate the effects of the presence of *Sal. ruber*
98 strains and viruses on the interactions and long-term phenotypic and genetic changes (evolution)
99 of *Sal. ruber* strain M1 and its M1EM1 virus (referred to as EM1 hereafter) (Fig. 1a). In experiment
100 1, *Sal. ruber* strain M1 was cultured alone. In experiment 2, *Sal. ruber* strains M8, M31, and P18
101 were added to the M1 culture. These two experiments served as virus-free controls. In experiment
102 3, M1 was infected with its EM1 virus. Experiment 4 included M1 infected with EM1, along with
103 the presence of strains M8, M31, and P18. Finally, experiment 5 included the same components
104 as experiment 4, with the addition of *Sal. ruber* M31CC1 and M31CR41-2 viruses (referred to as
105 CC1 and CR41-2, respectively), which infect both *Sal. ruber* strains M31 and M8, and M8CR-4
106 virus (i.e. CR4), which infects *Sal. ruber* strain M8 (Villamor et al., 2018) (Supplementary Table
107 1).

108 A short-term experiment, which included the first 9 days of incubation (corresponding to ~14
109 generations), evaluated several factors derived from the M1-EM1 infection process under different
110 contexts: lysis timing, virions produced, infective viruses and community dynamics. Thereafter,
111 all cultures were periodically transferred to fresh medium and maintained for 150 days. This
112 constituted the "long-term experiment", aimed at studying possible evolutionary changes in the
113 virus–host pair, while continuing to monitor key ecological and phenotypic parameters (Fig. 1b).

114 **Increased biological complexity leads to a delay in lysis of *Sal. ruber* M1 and a reduced**
115 **production of EM1 virions**

116 In the short-term experiment, *Sal. ruber* exhibited its characteristic growth pattern in experiments
117 1 and 2, with a slightly higher optical density (OD) in experiment 2 (Fig. 2a; Extended Data Fig.
118 1a). In infection experiment 3, lysis of *Sal. ruber* M1 was observed, followed by a recovery of the
119 population, a patter that mimic previous findings from our laboratory, in which that recovery was
120 mainly attributed to the emergence of pseudolysogens (Sanchez-Martinez et al., 2025). In
121 experiments 4 and 5, this OD recovery was observed earlier, which could be attributed to the
122 growth of uninfected strains.

123 The production of infectious EM1 viral particles, measured as plaque-forming-units (PFU) on *Sal.*
124 *ruber* M1, was significantly delayed in experiments 4 and 5 compared to experiment 3 (*t*-test p-
125 value < 0.0001) (Fig. 2b), indicating that the presence of additional *Sal. ruber* strains delayed the
126 lysis of strain M1 by the EM1 virus. After 96 hours, a decline in the number of infectious particles
127 was observed, more pronounced in experiments 4 and 5 than in experiment 3 (p-value < 0.01). In
128 all the experiments a slight decline in the number of PFUs was observed over time, with no
129 significant differences between experiments in the number of infectious EM1 viruses produced
130 between 6 and 9 days. Total extracellular virion concentration, measured by flow cytometry,
131 reached 9.7 x 10^{10} VLP/ml within 48 hours in experiment 3, whereas in experiment 4 this
132 concentration was 4.2 x 10^{8} VLP/ml, a statistically significant reduction (p-value < 0.0001) (Fig.
133 2c), consistent with the observations of PFU counts. Experiment 5 was excluded from this figure,
134 as the presence of multiple coexisting viruses prevents attributing VLP counts specifically to EM1
135 (Extended Data Fig. 1b).

136 High throughput microfluidics-based qPCR revealed that the concentration of the M1 strain
137 (measured as genomes/ml) varied across experiments and time points (Fig. 3a). At 48 hours, M1
138 abundance dropped significantly in experiment 3 (3.9 x 10^{6} genomes/ml), indicating active lysis
139 of the population, while it remained at higher numbers in experiments 4 (1.2 x 10^{9} genomes/ml)
140 and 5 (7.6 x 10^{8} genomes/ml) (p-value < 0.0001). By 72 hours, M1 levels decreased in all
141 experiments, maintaining low values in experiment 3 (3.8 x 10^{6} genomes/ml), and showing

142 delayed but evident reductions in experiments 4 and 5 (2.2 x 10^6 and 5.2 x 10^6 genomes/ml,
143 respectively) (Fig. 3a; Supplementary Fig. 1).

144 In the case of the bacterial community, in experiment 4 a decrease in the concentration of M8,
145 M31, and P18 strains was observed at 50 hours, despite the absence of their viruses (Fig. 3a). This
146 pattern suggests that the growth of these strains was transiently inhibited after *Sal. ruber* M1 lysis.
147 To test this, virus-free lysate from an M1-infected culture was added to pure cultures of M8, M31,
148 and P18. A clear, transient growth inhibition was observed, confirming that the M1 lysate affected
149 the growth of the other strains (Extended Data Fig. 2). Similar results have been reported in other
150 studies, where intracellular bacterial contents released upon lysis can inhibit the growth of other
151 bacteria (Penchuk et al., 2023; Smakman & Hall, 2022). In experiment 5, M8 showed minimal
152 growth. As the only strain infected by three viruses (Supplementary Table 1), M8 likely could not
153 withstand the high viral pressure, explaining its poor performance under these conditions.

154 Regarding the extracellular viruses measured by microfluidics-based qPCR, a lower concentration
155 of EM1 was observed at 48 hours in both experiments 4 and 5 (2.2 x 10^8 and 3.3 x 10^8 genomes/ml,
156 respectively) compared with experiment 3 (4.2 x 10^9 genomes/ml) (p-value < 0.0001) (Fig. 3b;
157 Supplementary Fig. 2), confirming that increased community complexity delays the infection and
158 lysis of *Sal. ruber* M1 by the EM1 virus. By 216 hours (day 9), experiment 4 yielded significantly
159 lower VLP concentration (2.4 x 10^{10} VLP/ml) than experiment 3 (2.8 x 10^{10} VLP/ml) (p-value <
160 0.05) (Fig. 2c). Microfluidics-based qPCR measurements also revealed that the concentration of
161 extracellular EM1 viruses in experiments 4 and 5 (7.6 x 10^9 and 3.4 x 10^9 genomes/ml,
162 respectively) was significantly lower than in experiment 3 (2.7 x 10^{10} genomes/ml) at the same
163 time point (p-value < 0.01), supporting the flow cytometry results (Fig. 3b). These findings
164 indicate that the presence of additional *Sal. ruber* strains reduced the overall production of EM1,
165 in good agreement with previous studies showing that the presence of other bacterial species can
166 lead to lower viral densities (Alseth et al., 2019; Mumford & Friman, 2017). In contrast, a recent
167 study found no differences in lysis timing or viral titers produced by *Pseudomonas aeruginosa*
168 PA14 when exposed to competing bacterial strains (Alseth et al., 2024).

169 Experiment 5 also revealed distinct patterns in the production of other extracellular viruses. CC1
170 virus, which infects both *Sal. ruber* M8 and M31, showed sustained high titers from 50 hours

171 onward, consistent with ongoing replication in its hosts (Fig. 3b). CR41-2 virus, which infects the
172 same strains as CC1 (M8 and M31), was only detected on days 1 and 4. Adsorption assays revealed
173 that CR41-2 adsorbs significantly less efficiently than CC1 to M31 (Supplementary Fig. 3). Thus,
174 CC1 may have outcompeted CR41-2 for access to M31, thereby limiting CR41-2 infection. This
175 observation aligns with a well-established principle of phage biology, that considers adsorption
176 efficiency as a critical determinant of successful phage infection and subsequent replication
177 (Abedon, 2023). Such virus–virus competition for shared hosts can strongly shape infection
178 dynamics, allowing more efficient viruses to suppress the adsorption of less competitive ones
179 (Bürkle et al., 2025; Turner, 2005). Finally, CR4 virus, which exclusively infects M8, exhibited
180 an early increase in viral concentration followed by a sharp decline (Fig. 3b). This decline likely
181 reflects the lack of M8 cell growth, which limited the availability of susceptible hosts and
182 consequently reduced further CR4 replication.

183 ***Sal. ruber* M1 and its EM1 virus establish a stable long-term relationship, regardless of the**
184 **biological context**

185 After the initial 9-day period, all cultures were transferred to fresh medium to monitor their long-
186 term evolution with transfers every 9-13 days over a total of 150 days (13 transfers in total,
187 corresponding to ~240 generations). At selected time points, specific parameters were assessed,
188 including changes in host range and infectivity toward the native host (Fig. 1b).

189 *Sal. ruber* M1 was maintained at high density (~10^9 genomes/ml) across all time points, regardless
190 of the presence of EM1 or other strains and viruses (Extended Data Fig. 3). The EM1 virus
191 maintained relatively stable concentrations extracellularly across all three experiments (Extended
192 Data Fig. 4; Supplementary Fig. 4). Although the EM1 titer declined by about one order of
193 magnitude between days 52 and 84, its level remained stable until the end of the study. These
194 results indicate that *Sal. ruber* M1 and its EM1 virus established a stable coexistence that persisted
195 throughout the study, regardless of the surrounding biological context. Long-term virus–host
196 coexistence has been widely reported in other systems driven by mechanisms such as arms-race
197 dynamics, spatial heterogeneity, or phase variation in gene expression (Cortés-Martín et al., 2025;
198 Kortright et al., 2022; Lourenço et al., 2020). However, a previous work from our group
199 demonstrated that EM1 can be maintained in *Sal. ruber* M1 in a pseudolysogenic state (Sanchez-

200 Martinez et al., 2025), which appears to underlie the stable coexistence observed here. Its
201 establishment and maintenance do not seem to be affected by the presence of additional strains
202 and viruses.

203 Additional insights emerged from the dynamics of the other community members. In experiment
204 5, CC1 remained at high concentrations, as well as one of their hosts, M31, which was also detected
205 until the end of the experiment (Extended Data Fig. 3 and 4). In the case of the CR4 virus, although
206 it was not detected extracellularly after 9 days, it persisted in the total culture until 84 days,
207 coinciding with the extinction of its host M8 (Supplementary Fig. 4). The P18 strain, the only one
208 not infected by any virus, disappeared in experiment 5 from all 3 replicates and, although still
209 detectable, was outcompeted by other strains in experiments 2 and 4. This indicates that viruses
210 were not the only force structuring the community, and that competitive interactions among
211 bacterial strains also played a crucial role.

212 **The biological context reduces the infectivity of the EM1 virus and alters its host range**

213 On day 9, the infectivity of EM1, calculated as the ratio between PFU/ml (tested with the native
214 M1 strain as the host) and extracellular EM1 genomes/ml, was maintained above 0.1% in the three
215 experiments and remained stable at these levels for 52 days (Fig. 4a). However, by day 84,
216 significant differences (p-value < 0.0001) emerged between experiment 3 and experiments 4 and
217 5. In experiment 3 infectivity remained stable but, in experiment 4, where the *Sal. ruber* M1-EM1
218 pair was accompanied by other strains, infectivity dropped by almost one order of magnitude. In
219 experiment 5, the most biologically complex, this reduction in infectivity was more drastic, with a
220 drop of nearly 4 orders of magnitude compared to experiment 3. By day 130, infectivity had
221 decreased further in all experiments, down to 5 orders of magnitude below the initial level. These
222 findings suggested that the EM1 virus underwent genomic changes, as further explored below,
223 which reduced its ability to infect the native strain in all the experiments and highlighted that the
224 biological context significantly affected the interactions between EM1 and its host.

225 Host range changes were also detected in the EM1 virus in experiment 5, whereas no such changes
226 were observed in experiments 3 and 4. The evolved EM1 in experiment 5, which initially only
227 infected the M1 strain, expanded its host range and infected the native M8 strain consistently across
228 all three biological replicates at 84 hours (Fig. 4b). Several studies have reported host range

229 changes in simplified experimental evolution contexts (Bono et al., 2015; Holtzman et al., 2020;
230 Sant et al., 2021; Subramanian et al., 2022), but only a few have explored this phenomenon under
231 more complex conditions. In multispecies settings, viruses have been shown to broaden their host
232 range by transiently using alternative hosts as intermediates to access new hosts (De Sordi et al.,
233 2017), which may partly explain why this host range shift occurred in experiment 5. Moreover, it
234 has been observed that the presence of multiple viruses affect the host range of a given virus by
235 driving evolutionary changes of the host that affect its susceptibility (Avrani et al., 2011;
236 Chevallereau et al., 2022). These findings suggest that the observed host range expansion in EM1
237 was a result of selective pressures arising from increased ecological complexity. Coexistence with
238 other strains and viruses may have favored viral variants capable of infecting alternative hosts (i.e.,
239 either by exploiting new receptor variants or by overcoming host-specific resistance mechanisms
240 (see below)). In the case of the other viruses, none of them showed any host range changes.

241 The unequal decline in the EM1 virus infectivity across experiments, together with the shift in host
242 range observed in experiment 5, suggested that EM1 underwent different genomic changes under
243 the different conditions, influencing the virus–host evolutionary trajectory according to the
244 surrounding biotic environment. To analyze whether genomic changes could be responsible for
245 these differences, extracellular viromes and cellular pellets from experiments 3, 4 and 5 were
246 sequenced on days 9, 84 and 150. The original viral genomes were also sequenced as references.

247 **Viral genomic diversification is enhanced by the presence of other viruses**

248 EM1 genome remained largely stable during the early stages of the experiment, with only a single
249 mutation in a gene coding for a hypothetical protein detected across all treatments by day 9
250 (Supplementary Table 2). By day 84, mutation accumulation remained low in experiments 3 and
251 4 (15 and 14 mutations, respectively), mostly in non-coding regions (Extended Data Fig. 5;
252 Supplementary Table 2). Experiment 5 showed a markedly different pattern, with 772 mutations
253 distributed across the genome. A large proportion of these occurred in structural genes, particularly
254 those related to tail components. Two minor tail protein genes accumulated over 190 mutations,
255 and a long-tail fiber protein gene showed 69 changes, suggesting strong selective pressure on host
256 recognition machinery. This genomic diversification coincided with a sharp drop in EM1

257 infectivity against the native M1 host, pointing to a possible link between mutation accumulation
258 in tail-related regions and host range evolution.

259 As the experiment progressed to day 150, the accumulation of mutations continued to diverge
260 between treatments. Experiment 3 reached a total of 34 mutations, including 17 in a gene coding
261 for a DNA methyltransferase and several nonsynonymous changes in genes for a DNA-binding
262 protein, a minor tail protein, and a long-tail fiber protein, some of which may be linked to the
263 observed decline in infectivity (Fig. 5). Experiment 4 accumulated 267 mutations, with a high
264 concentration in genes related to DNA metabolism, such as a DNA primase and a single-strand
265 DNA-binding protein. This accumulation of mutations in DNA metabolism-related genes could
266 suggest a potential disruption in viral replication, contributing to reduced infectivity (Boddin et al.,
267 2022; Jiang et al., 2007, 2009). In experiment 5, mutation accumulation intensified, reaching 1,331
268 mutations distributed across the genome. Structural and replication-related genes showed
269 particularly high mutational loads, including 198 mutations in minor tail protein genes and over
270 190 combined in genes for a DNA-binding protein and a DNA primase. This translated into a
271 mutation rate of 2.5×10^{-4} mutations per site per day in experiment 5, markedly higher than those
272 estimated for experiments 3 and 4 (6.4×10^{-6} and 5×10^{-5}, respectively) (Supplementary Table 2).

273 These differences were reflected in the average nucleotide identity of sequence alignment reads
274 (ANIr) along the EM1 genome (the mean nucleotide-level similarity between mapped reads and
275 the reference genome). Experiments 3 and 4 showed higher ANIr values (99.70% and 99.75%,
276 respectively) indicating a more homogeneous population, compared to experiment 5 (98.13%) on
277 day 150 (Supplementary Table 2). The lower ANIr values observed in the presence of other viruses
278 indicated an accelerated diversification of the viral population, with the emergence of multiple
279 distinct genotypes or "genomovars" (defined as variants with ANI <99.5%) (Aldeguer-Riquelme
280 et al., 2024).

281 The increase in genetic variability observed under complex community conditions reveals a
282 previously overlooked role of viral coexistence in promoting diversification. Our results
283 demonstrate that the mere presence of other viruses can substantially reshape the genetic structure
284 of a viral population, both in terms of mutation rate and the distribution of these mutations across
285 the genome (Supplementary Table 2; Fig. 5). This diversification was accompanied by a drastic

286 loss of infectivity and a shift in host range, likely driven by mutations in tail protein genes. While
287 previous studies have shown that viral mutation rates can vary depending on the host genotype
288 (Duffy, 2018; Longdon et al., 2014; Sant et al., 2021), and that exposure to multiple host genotypes
289 can promote tail gene diversification (Hernandez et al., 2024), our findings suggest a previously
290 unreported mechanism. Here, it is the presence of other viruses, more than the mere presence of
291 other hosts, that significantly increased the viral mutation rate. This uncovers a novel form of
292 virus–virus interaction, where coexisting viruses indirectly drive each other's evolutionary
293 trajectories. Such interactions, largely overlooked to date, could play a central role in shaping viral
294 evolution in natural communities characterized by high viral diversity.

295 **Intracellular viral diversity exceeds the subset released extracellularly**

296 Analysis of intracellular populations revealed that only part of the viral diversity generated inside
297 host cells was released extracellularly, indicating that the extracellular fraction corresponds to a
298 selected subset of intracellular genotypes (i.e., viruses maintained episomally and/or genomes
299 undergoing replication for virion packaging). Three genes (marked with an asterisk in Fig. 5) were
300 characterized by amplicon sequencing: one encoding a hypothetical protein with minimal
301 mutations across all experiments (used as a control), and two genes highly mutated in experiment
302 5, encoding a minor tail protein and a DNA-binding protein, respectively. The mutation patterns
303 in these genes were generally similar to those observed in the extracellular viral population,
304 especially in experiments 3 and 4, with few differences (Extended Data Fig. 6). Experiment 5
305 displayed a markedly higher number of mutations in the intracellular fraction in both the minor
306 tail protein and DNA-binding protein genes (63 and 30 mutations on average across replicates)
307 compared to experiment 3 (0 and 2 mutations) and experiment 4 (no mutations).

308 When comparing intracellular and extracellular fractions some differences emerged, particularly
309 in experiment 5. Both the minor tail protein and DNA-binding protein regions showed a high
310 number of mutations at nearly 100% frequency in the extracellular fraction, while the intracellular
311 fraction exhibited greater heterogeneity in mutation frequencies. These results support our earlier
312 findings that the presence of other viruses acts as a selective force, increasing the mutation rate of
313 EM1 and generating a larger diversity of viral genotypes. However, based on the intracellular data,

314 only a subset of these genotypes appears to be selected and successfully replicated for virion
315 production.

316 **Intraspecific interactions, rather than viral pressure, drive host genome evolution**

317 We also analyzed genetic mutations in the host *Sal. ruber* M1. As experiments 2, 4, and 5 included
318 additional *Sal. ruber* strains sharing large genome regions, we focused on nine genomic regions,
319 ranging from 1.8 to 23.5 kb, specific to *Sal. ruber* M1. This strategy allowed us to unambiguously
320 track mutations in M1 despite the presence of other closely related strains in the mixed cultures.
321 In total, 70.1 kb were analyzed, (Supplementary Fig. 5). Mutation counts at 150 hours revealed
322 striking differences: 9 mutations in experiment 1, 224 in experiment 2, 8 in experiment 3, 266 in
323 experiment 4, and 14 in experiment 5, with most occurring in non-coding regions (Extended Data
324 Fig. 7; Supplementary Table 3). These findings corresponded to mutation rates of 7,6 x 10^{-7}, 2,1 x
325 10^{-5}, 6,7 x 10^{-7}, 5 x 10^{-5}, 5,6 x 10^{-6} mutations per site per day, respectively (Supplementary Table
326 3). Our results demonstrate that *Sal. ruber* M1 experienced significantly elevated mutation rates
327 in specific regions in those experiments where it evolved alongside multiple strains—experiments
328 2 and 4 (Extended Data Fig. 3).

329 In contrast, experiment 5, which also included other viruses, resulted in markedly lower host
330 mutation rates. This suggests that the presence of viruses in a complex community context may
331 constrain bacterial evolution, rather than accelerate it. This finding is striking and counterintuitive,
332 as viruses are typically considered potent drivers of evolutionary change, and other studies showed
333 that bacteria coevolving with multiple viruses exhibited higher mutation rates (Betts et al., 2018;
334 Wielgoss et al., 2016). In our system, however, viral pressure may have limited evolutionary
335 change in the host, possibly by imposing bottlenecks through lysis, constraining population
336 dynamics, or reducing the strength of competition among bacterial strains.

337 The observed increase in mutation rates under competitive conditions suggests that bacterial
338 intraspecific competition is a strong driver of genomic evolution in the host. While EM1 viral
339 mutations primarily emerged within infected populations, *Sal. ruber* M1 genetic variability was
340 predominantly shaped by interactions with coexisting bacterial strains. This is consistent with
341 previous work from our laboratory demonstrating weak but significant competitive interactions
342 between *Sal. ruber* strains in co-culture (Peña et al., 2010). Furthermore, in a recent mesocosm

experiment, we showed that strain M8 was displaced by other genotypes after being introduced at high abundance into a pond, suggesting competitive exclusion through intraspecific competition (Ramos-Barbero et al., 2024).

Several mechanisms could account for the elevated mutation rates observed in experiments 2 and 4. These include stress-induced mutagenesis, where competition triggers cellular stress responses that increase mutation frequency (Svet et al., 2023; Trejo-Hernández et al., 2014), and the selection of hypermutator phenotypes (bacterial variants with defective DNA repair systems) previously documented in *Escherichia coli* during gut colonization (Giraud et al., 2001) and *Vibrio cholerae* under antibiotic pressure (Baharoglu & Mazel, 2011). In our system, the sharp increase in mutations specifically in the absence of viral pressure suggests that competition with other bacterial strains may trigger stress responses or transient mutagenic states, rather than the stable fixation of hypermutator lineages. This is further supported by the fact that mutation rates remained low in experiment 5, despite the presence of both other strains and viruses, indicating that viral pressure may counteract or suppress the effects of competition-induced mutagenesis.

These findings support the view that microbial competition plays a central role in shaping evolutionary trajectories. Together, they underscore a critical consideration for evolutionary studies: microbial mutation rates and adaptation cannot be fully understood without accounting for the complex network of interspecies interactions that govern microbial life in natural environments.

CONCLUSIONS

The usefulness of studying virus–host interactions within microcosms that simulate natural conditions in a stepwise manner has become increasingly evident in recent years (Blazanin & Turner, 2021; Castledine & Buckling, 2024; Chevallereau et al., 2022; Koskella et al., 2022). Understanding the ecological and evolutionary dynamics of viruses and prokaryotes in their natural environments not only enriches our knowledge of the natural world but also enables us to manipulate these communities more predictably. In this study, we demonstrate that a semi-

370 complex biological context (encompassing *Sal. ruber* strains and their viruses) substantially
371 influence the ecology and evolution of the *Sal. ruber* M1-EM1 pair in controlled microcosms.

372 This work shows how in the short-term, the presence of additional *Sal. ruber* strains delays the
373 lysis of *Sal. ruber* M1 and reduces EM1 virion production. These effects were consistent across
374 different quantification methods, indicating that community composition has a measurable impact
375 on virus replication dynamics. In the long-term, *Sal. ruber* M1 and the EM1 virus established a
376 stable coexistence throughout the entire experiment regardless of community complexity. The
377 infectivity of EM1 against its original host declined faster in the presence of other viruses,
378 revealing that viral genomic diversification is enhanced by virus–virus interactions. This reduction
379 in infectivity was linked to genomic changes in EM1, leading to an expanded host range and a
380 sharply increased mutation rate in the presence of other viruses. Meanwhile, the bacterial host, *Sal.*
381 *ruber* M1, showed elevated mutation rates evolving alongside other strains, indicating that
382 intraspecific bacterial interactions—not viral pressure—drive host genome evolution.

383 Overall, our results highlight the critical importance of incorporating biological complexity in
384 studies of virus–host interactions. These findings emphasize the need to consider the multifaceted
385 nature of microbial communities to more accurately predict virus–host dynamics and their
386 ecological and evolutionary consequences in natural environments.

387

388 **METHODS**

389 **Bacterial strains, viruses and experimental design**

390 *Sal. ruber* strains M1, M8, M31 and P18 were aerobically grown with gentle shaking (60 rpm) at
391 37ºC in 25 % SW (sea water, a salt solution containing the salts present in seawater at a total
392 concentration of 25% weight/volume) with 0.2 % yeast extract (Rodriguez-Valera et al., 1985).
393 *Sal ruber* viruses used in this study, named M1EM-1, M31CC-1, M8CR-4 and M31CR41-2
394 (referred to here as EM1, CC1, CR4 and CR41-2, respectively, for convenience), were isolated
395 during a previous study in our laboratory (Villamor et al., 2018).

396 Five experiments were conducted in parallel (Fig. 1). In all the experiments, 25 ml of culture media
397 were inoculated with $7.5x10^8$ cells of *Sal. ruber* M1. In experiments 2, 4, and 5, the cultures also
398 included 2.5×10^7 cells of each of the M8, M31, and P18 strains. In experiments 3, 4 and 5, $7.5x10^7$
399 virus-like particles (VLP) of the strictly virulent EM1 virus (multiplicity of infection = 0.01),
400 which only infects the M1 strain, were added. Experiment 5 also contained $2.5x10^6$ VLP of each
401 one of the CC1, CR4 and CR41-2 viruses that infect M8 and M31 strains (Supplementary Table
402 1). After inoculation, experiments were incubated for 9 days as described above, taking aliquots
403 once a day for culture monitoring by optical density (OD) at 600 nm and additional approaches
404 (see below). This was defined as the short-term experiment.

405 On day 9 (213 hours after inoculation), 250 µl of each experiment were transferred to 25 ml of
406 fresh medium and incubated as described above. After 13 days, new aliquots were collected to
407 quantify the bacterial and viral diversity of the cultures by microfluidics-based qPCR (see below)
408 and transferred and incubated in the same way. This was repeated every approximately 9-13 days
409 for 150 days. Days 9 to 150 were considered as the long-term experiment.

410 In addition, on days 9, 52, 84, 130 and 150, aliquots were taken for plaque forming units (PFU)
411 quantification, host range analyses of the viruses and DNA extraction and sequencing. All
412 experiments were conducted in triplicate.

413 **Flow cytometry**

414 For each day of the short-term experiment, cells/ml and VLP/ml were quantified by flow cytometry
415 as described in Brussaard, 2004. Briefly, 500 µl of each sample were fixed with glutaraldehyde
416 (0.5% final concentration) at 4ºC for 30 min, flash-frozen in liquid nitrogen, and stored at -80°C
417 until use. Upon thawing, samples were diluted in Tris-EDTA buffer (pH 8), stained with
418 SYBR™Gold (0.5X final concentration), incubated for 10 min in the dark at 80°C, and cooled for
419 5 min at room temperature prior to analysis.

420 The cytometer settings were as follows: the threshold was set in blue fluorescence (300 units),
421 FITC voltage = 500, SSC voltage = 300, forward scatter voltage = 500, and the flow rate was
422 established as low (15 µl/min). Background noise was checked on blanks, composed by TE buffer
423 stained with SYBR Gold. Samples were recorded with an event rate of 100-1000 events per second.

424 Cells and VLP counts were obtained by correcting the background measured in blanks. Cells and
425 VLP abundances were respectively expressed as cells/ml or VLP/ml.

426 **Plaque assay**

427 The number of free infective EM1 viruses at each sampling point of the short- and long-term
428 experiments was determined by plaque assay in experiments 3, 4 and 5. Aliquots of 150 µl were
429 centrifuged at 17,000 x g for 10 min and supernatants were serially diluted in sterile SW 25%. 100
430 µl of dilutions 10^{-4}, 10^{-6} and 10^{-8} were mixed with 500 µl of *Sal. ruber* M1 in exponential phase.
431 Four ml of soft agar (25% SW with 0.2% yeast extract and 0.7% agar) were added and this was
432 poured on plates with solid media. After the agar had solidified, the plates were incubated at 37ºC
433 for 10 days until plaques were visible. The number of free infective viruses (PFU/ml) was counted
434 and represented. On days 9, 52, 84, 130 and 150, plaque assays were also carried out to obtain
435 individual plaques of all viruses for experiment 5, using as hosts the native strains M8, M31 and
436 P18.

437 **High throughput microfluidics-based qPCR**

438 Individual targets (i.e. the 4 strains and the 4 viruses) were quantified in each point of the short-
439 term experiment, in both the total culture and the supernatant to quantify free viruses, using the
440 Biomark HD high throughput microfluidics-based qPCR system (Standard Biotools, South San
441 Francisco, USA). Primers for each target gene were designed using using Geneious software 6.1.8
442 (Biomatters, Auckland, New Zealand) (Supplementary Table 4). From each of the experiments,
443 100 µl of the culture were taken for total culture analysis and 120 µl for supernatant quantification
444 of free viruses. In the latter, a centrifugation step consisting of 10 min at 7,197 x g and 100 µl
445 supernatant transfer to a clean eppendorf tube was performed. Both were fixed with 0.5% (final
446 concentration) of formaldehyde for 1 hour at 4°C, diluted 10-fold in phosphate buffered saline
447 (PBS) 1X, and stored at 4°C.

448 DNA targets were then pre-amplified using the PreAmp Master Mix (Standard Biotools, South
449 San Francisco, USA) following manufacturer's instructions. In brief, a primer pool was prepared
450 by mixing the forward and reverse primers for all targets (Supplementary Table 4) and diluting the
451 mixture with DNA suspension buffer (10 mM Tris/HCL and 0.1 mM EDTA pH 8) to a final

452 concentration of 0.5 µM of each primer pair. Each sample was then pre-amplified in a total volume
453 of 5 uL containing 1 µL PreAmp Master Mix (Standard Biotools, South San Francisco, USA),
454 0.5 µL of primer pool and 3.5 µL of sample. Preamplification reactions were performed on a
455 Simpliamp Thermal Cycler (Applied Biosystems, Waltham, USA) using the following sample
456 conditions: an initial activation cycle at 95°C for 10 min followed by 14 two-step cycles
457 (denaturation at 95°C for 15 seconds and annealing/extension at 60°C for 4 min). The preamplified
458 products were subjected to Exonuclease I cleanup (New England Biolabs, Massachusetts, USA)
459 to remove any unincorporated primers (4 U/µL final concentration at 37°C for 30 min followed by
460 inactivation at 80ºC for 15 min). A 1:5 dilution using DNA suspension buffer was then performed
461 on the Exonuclease I treated samples and stored at -20°C.

462 Finally, pre-amplified DNA targets were quantified by microfluidics-based qPCR on 192x24
463 Dynamic Array™ IFCs (Fluidigm, South San Francisco, USA) according to manufacturer's
464 instructions. In brief, 10X assay primer mixtures for each DNA target and sample pre-mixes for
465 each sample were prepared in triplicate. For the generation of the 10X assay primer mixtures, the
466 forward and reverse primers for a single DNA target were pooled together at a concentration of 50
467 uM each. 0.15 uL of this pool were then mixed with 1.35 µl of DNA suspension buffer (Tris/HCL
468 and 0.1 mM EDTA pH 8) and 1.5 µl of 2X Assay Loading Reagent (Standard Biotools, South San
469 Francisco, USA). Sample pre-mixes were made by combining 1.5 µl SsoFast™ Evagreen®
470 Supermix 2X (BioRad, California, USA) with 0.15 µl 20X GE Sample Loading Reagent (Standard
471 Biotools, South San Francisco, USA) and 1.35 µl of pre-amplified DNA. The 192x24 Dynamic
472 Array™ IFCs were then primed on a Juno controller (Standard Biotools, South San Francisco,
473 USA) and 3 uL of each 10X assay primer mix and sample pre-mix were transferred to the
474 appropriate inlets of the IFC and loaded using again the Juno controller. After loading, the IFC
475 was transferred to a Biomark HD instrument (Standard Biotools, South San Francisco, USA) and
476 qPCR reactions were performed using the following cycling conditions: 95°C for 1 min, followed
477 by 30 two-step cycles (95°C for 15 seconds and 60°C for 20 seconds) and a final melt curve
478 analysis. Data were analyzed with the Real-Time PCR Analysis Software (Standard Biotools,
479 South San Francisco, USA) using manually defined thresholds. All samples were run in triplicate
480 (including the standards and negative controls). All samples, standards, and negative controls were
481 run in triplicate, with negative controls included both in the pre-amplification and in the
482 microfluidics-based qPCR. A total of four 192x24 Dynamic Array™ IFCs were used, each with

483 its own standard curve consisting of five concentration points for every target, and each chip
484 included positive controls for the eight targets individually.

485 **Host range through spot test and qPCR**

486 The host range of each virus at time 0 was determined through a spot test. Briefly, 4 ml of molten
487 0.7% top agar of 25% SW with 0.2% yeast extract were mixed with 500 µl of bacterial cultures at
488 exponential phase and plated on solid medium. Once solidified, 3 µl of each virus, titered at 10^{10}
489 PFUs/ml and diluted 10^2, 10^4 and 10^6 times, were added to the corresponding lawn. The spotted
490 plates were left to dry and incubated at 37ºC for 10 days. The detection of a clearance zone was
491 interpreted as evidence of viral lysis while the areas exhibiting growth were attributed to resistance.
492 This was done by exposing the 4 native strains (*Sal. ruber* strains M1, M8, M31 and P18) to the 4
493 viruses (EM1, CC1, CR41-2 and CR4 viruses).

494 The viral fractions from experiments 3, 4 and 5, at 9, 52, 84, 130 and 150 days, were obtained by
495 centrifuging each replicate at 7,197 x g for 20 min and filtering the supernatant through a 0.22 µm
496 filter (Millipore, Burlington, USA). For experiments 3 and 4, the host range of the EM1 virus over
497 time was measured through a spot test against the 4 native hosts as described above.

498 The determination of the host range of the 4 viruses over time in experiment 5 was performed by
499 qPCR as follows. All the plaques obtained for each native host (see plaque assay above) for each
500 replicate on days 9, 52, 84, 130 and 150, were picked from the soft agar and resuspended in 1 ml
501 of ultrapure water. The presence of each virus in these mixtures of plaques were checked by qPCR
502 with specific primers (Supplementary Table 4) using SYBR Green. The experiment was carried
503 out with the standard run in a StepOnePlus PCR System (Life Technologies, Carlsbad, USA) in a
504 10 µl reaction mixture with Power SYBR Green PCR Master Mix (Applied Biosystems, Waltham,
505 USA). The reaction contained: 5 µl of 2X Master Mix, 0.2 µl of each 10 µM primer, 1 µl of sample
506 and ultrapure water to complete volume. Conditions are detailed in Supplementary Table 5. The
507 results were analyzed with the Applied Biosystems StepOne™ Instrument program. All samples
508 were run in triplicate (including the standards and negative controls).

509 **Adsorption assay**

510 An adsorption assay was performed in parallel with the CC1 and CR41-2 viruses and *Sal. ruber*
511 M31 wild type. Cultures in exponential phase were diluted with fresh medium to an OD of 0.3 and
512 $2x10^8$ cells were mixed with $2x10^6$ PFU (MOI=0.01) of the virus. This was considered as the initial
513 time. Mixtures were then incubated at 37 ºC and 60 rpm. Aliquots of 150 µl were taken along 5 h
514 (at 1, 2, 3, 4 and 5 h), centrifuged at 17,000 x g for 8 min, and 120 µl of the cells-free supernatant
515 were stored in ice. The numbers of PFU/ml were measured by plaque assay as described above.
516 All the experiments were conducted in triplicate.

517 **Lysate experiment**

518 An infection of *Sal. ruber* M1 with the EM1 virus at a MOI of 0.1 was carried out under the same
519 conditions as described above. After 5 days, the infection was centrifuged at 17,000 x g for 10
520 minutes, and the supernatant was filtered through a 0.022 µm filter (Millipore, Burlington, USA)
521 to remove any remaining viruses. One ml of this lysate was added to 25 ml of exponential-phase
522 cultures of M8, M31, and P18 strains. Controls received 1 ml of fresh medium instead. Optical
523 density was measured at 600 nm. Both the lysate-treated cultures and controls were conducted in
524 triplicate.

525 **DNA extractions and sequencing**

526 The three biological replicates of each experiment were pooled prior to DNA extraction, as
527 previous experiments in our laboratory have shown high reproducibility in the mutational
528 trajectories of replicate populations. Bacterial pellets from all the experiments at 150 days were
529 obtained by centrifugation at 17,000 x g for 10 min. The cells were washed with sterile medium,
530 the supernatant removed, and the cell pellets stored at -80ºC until extraction. DNA was extracted
531 with the DNeasy Blood & Tissue Kit (Qiagen, Hilden, Germany) following the manufacturer's
532 protocol, and nucleic acids eluted in 70 µL of ultrapure water.

533 Viruses from the same points were obtained by centrifuging at 7.197 x g for 20 min and filtering
534 the supernatant through a filter of 0.22 µm. Dissolved DNA was removed with DNAse I from
535 bovine pancreas (Sigma-Aldrich, St. Louis, USA) at 37ºC for 30 min, with an inactivation at 75ºC
536 for 10 min. DNA was extracted with the QIAamp MinElute Virus Kit (Qiagen, Hilden, Germany)

537 following the manufacturer's protocol, and nucleic acids eluted in 35 µL of ultrapure water. DNA
538 from the viruses used for infecting at the initial time was also extracted as a reference.

539 All extracted cellular and viral DNAs were quantified using Qubit 2.0. Flourometer (Life
540 Technologies, Carlsbad, USA), and sequenced on an Illumina Novaseq6000 (2 x 150 bp) at
541 Macrogen (Macrogen, Seoul, South Korea).

542 **Metabarcoding**

543 Three genes from the EM1 virus were selected, and specific primers targeting ~375 bp regions
544 were designed (Supplementary Table 6). Cell pellets were washed three times by centrifugation,
545 and DNA was extracted and quantified as described above. Specific regions were amplified via
546 PCR in 50 µL reactions containing: 1.5 mM $MgCl_2$, 10X buffer, 10 mM dNTPs, 5 U/µL Taq
547 polymerase, 100 µM primers, 5 µg of the template DNA and water up to the volume. PCR
548 conditions are detailed in Supplementary Table 7. Five ml of the amplified products were
549 electrophoresed, stained with ethidium bromide (100 µg/mL), and visualized under UV light. The
550 remaining product was sequenced on an Illumina Miseq (2 x 150 bp) at Fundació per al Foment
551 de la Investigació Sanitària i Biomèdica de la Comunitat Valenciana (Fisabio, Valencia, Spain).

552 Mutations were identified comparing the obtained reads with the reference genomes of the viruses
553 at initial time using Geneious software 6.1.8 (Biomatters, Auckland, New Zealand) with a
554 minimum variant frequency of 0.01% and a coverage >50% to the mean coverage. Mutations were
555 represented using the package 'ggplot2' v3.4.0 in R v4.2.2.

556 **Bioinformatic analysis**

557 Primers and adapters were removed from sequences, and reads were filtered based on quality
558 scores using Trimmomatic v0.36.0 (Bolger et al., 2014). Trimmed reads of initial viruses were
559 assembled using SPAdes v3.13.1 (Bankevich et al., 2012) with the trusted option using their
560 genomes of NCBI as a reference (GenBank accession numbers MF580955, MF580958,
561 MF580960 and MF580960).

562 Mutations generated in the viruses over time were identified by comparing reads from the
563 extracellular viromes on days 9, 84 and 150 with the reference genomes of the viruses at initial

time using Geneious software 6.1.8 (Biomatters, Auckland, New Zealand) with a minimum variant frequency of 0.01% and a coverage >50% to the mean coverage. Mutations were represented using the package 'ggplot2' v3.4.0 in R v4.2.2. For the analysis of M1 sequences, the chromosomes of strains M1, M8, M31 and P18 were aligned with Mauve (Darling et al., 2004) and 9 M1-specific regions were selected where the mutations were called in the same way as for the virus.

A BLASTn was performed with the reads of each virome, using the genome of the EM1 virus as the reference. Then, the BLASTn output was filtered by best_hit option and read coverage >70%. The ANIr (average nucleotide identity of sequence alignment reads) along the genome of EM1 was calculated with a home-made script in windows of 50 bp and plotted. Recruitment plots were carried out by enveomics tool (Rodriguez-R & Konstantinidis, 2016) using enve.recplot 2 (R stadistic pluging).

REFERENCES

Abedon, S. T. (2023). Bacteriophage Adsorption: Likelihood of Virion Encounter with Bacteria and Other Factors Affecting Rates. Antibiotics, 12(4), Article 4. https://doi.org/10.3390/antibiotics12040723

Aldeguer-Riquelme, B., Conrad, R. E., Antón, J., Rossello-Mora, R., & Konstantinidis, K. T. (2024). A natural ANI gap that can define intra-species units of bacteriophages and other viruses. mBio, 15(8), e01536-24. https://doi.org/10.1128/mbio.01536-24

Alseth, E. O., Custodio, R., Sundius, S. A., Kuske, R. A., Brown, S. P., & Westra, E. R. (2024). The impact of phage and phage resistance on microbial community dynamics. PLOS Biology, 22(4), e3002346. https://doi.org/10.1371/journal.pbio.3002346

Alseth, E. O., Pursey, E., Luján, A. M., McLeod, I., Rollie, C., & Westra, E. R. (2019). Bacterial biodiversity drives the evolution of CRISPR-based phage resistance. Nature, 574(7779), 549-552. https://doi.org/10.1038/s41586-019-1662-9

Antón, J., Oren, A., Benlloch, S., Rodríguez-Valera, F., Amann, R., & Rosselló-Mora, R. (2002). *Salinibacter ruber* gen. Nov., sp. Nov., a novel, extremely halophilic member of the Bacteria from

591 saltern crystallizer ponds. International Journal of Systematic and Evolutionary Microbiology,
592 52(2), 485-491. https://doi.org/10.1099/00207713-52-2-485

593 Avrani, S., Wurtzel, O., Sharon, I., Sorek, R., & Lindell, D. (2011). Genomic island variability
594 facilitates *Prochlorococcus*–virus coexistence. Nature, 474(7353), 604-608.
595 https://doi.org/10.1038/nature10172

596 Baharoglu, Z., & Mazel, D. (2011). *Vibrio cholerae* Triggers SOS and Mutagenesis in Response
597 to a Wide Range of Antibiotics: A Route towards Multiresistance. Antimicrobial Agents and
598 Chemotherapy, 55(5), 2438-2441. https://doi.org/10.1128/aac.01549-10

599 Bankevich, A., Nurk, S., Antipov, D., Gurevich, A. A., Dvorkin, M., Kulikov, A. S., Lesin, V. M.,
600 Nikolenko, S. I., Pham, S., Prjibelski, A. D., Pyshkin, A. V., Sirotkin, A. V., Vyahhi, N., Tesler,
601 G., Alekseyev, M. A., & Pevzner, P. A. (2012). SPAdes: A New Genome Assembly Algorithm
602 and Its Applications to Single-Cell Sequencing. Journal of Computational Biology, 19(5), 455-
603 477. https://doi.org/10.1089/cmb.2012.0021

604 Benton, T. G., Solan, M., Travis, J. M. J., & Sait, S. M. (2007). Microcosm experiments can inform
605 global ecological problems. Trends in Ecology & Evolution, 22(10), 516-521.
606 https://doi.org/10.1016/j.tree.2007.08.003

607 Betts, A., Gray, C., Zelek, M., MacLean, R. C., & King, K. C. (2018). High parasite diversity
608 accelerates host adaptation and diversification. Science, 360(6391), 907-911.
609 https://doi.org/10.1126/science.aam9974

610 Blazanin, M., & Turner, P. E. (2021). Community context matters for bacteria-phage ecology and
611 evolution. The ISME Journal, 15(11), 3119-3128. https://doi.org/10.1038/s41396-021-01012-x

612 Boddin, J., Ip, W.-H., Wilkens, B., von Stromberg, K., Ching, W., Koyuncu, E., Bertzbach, L. D.,
613 & Dobner, T. (2022). A Single Amino Acid Switch in the Adenoviral DNA Binding Protein
614 Abrogates Replication Center Formation and Productive Viral Infection. mBio, 13(2), e00144-22.
615 https://doi.org/10.1128/mbio.00144-22

616 Bolger, A. M., Lohse, M., & Usadel, B. (2014). Trimmomatic: A flexible trimmer for Illumina
617 sequence data. Bioinformatics, 30(15), 2114-2120. https://doi.org/10.1093/bioinformatics/btu170

618 Bono, L. M., Gensel, C. L., Pfennig, D. W., & Burch, C. L. (2015). Evolutionary rescue and the
619 coexistence of generalist and specialist competitors: An experimental test. Proceedings of the
620 Royal Society B: Biological Sciences, 282(1821), 20151932.
621 https://doi.org/10.1098/rspb.2015.1932

622 Brussaard, C. P. D. (2004). Optimization of Procedures for Counting Viruses by Flow Cytometry.
623 Applied and Environmental Microbiology, 70(3), 1506-1513.
624 https://doi.org/10.1128/AEM.70.3.1506-1513.2004

625 Bürkle, M., Korf, I. H. E., Lippegaus, A., Krautwurst, S., Rohde, C., Weissfuss, C., Nouailles, G.,
626 Tene, X. M., Gaborieau, B., Ghigo, J.-M., Ricard, J.-D., Hocke, A. C., Papenfort, K., Debarbieux,
627 L., Witzenrath, M., Wienhold, S.-M., & Krishnamoorthy, G. (2025). Phage–phage competition
628 and biofilms affect interactions between two virulent bacteriophages and *Pseudomonas*
629 *aeruginosa*. The ISME Journal, 19(1), wraf065. https://doi.org/10.1093/ismejo/wraf065

630 Burns, D. G., Janssen, P. H., Itoh, T., Kamekura, M., Li, Z., Jensen, G., Rodríguez-Valera, F.,
631 Bolhuis, H., & Dyall-Smith, M. L. (2007). *Haloquadratum walsbyi* gen. Nov., sp. Nov., the square
632 haloarchaeon of Walsby, isolated from saltern crystallizers in Australia and Spain. International
633 Journal of Systematic and Evolutionary Microbiology, 57(2), 387-392.
634 https://doi.org/10.1099/ijs.0.64690-0

635 Calisi, R. M., & Bentley, G. E. (2009). Lab and field experiments: Are they the same animal?
636 Hormones and Behavior, 56(1), 1-10. https://doi.org/10.1016/j.yhbeh.2009.02.010

637 Castledine, M., & Buckling, A. (2024). Critically evaluating the relative importance of phage in
638 shaping microbial community composition. Trends in Microbiology, 32(10), 957-969.
639 https://doi.org/10.1016/j.tim.2024.02.014

640 Chen, J., Zhang, Y., Kuzyakov, Y., Wang, D., & Olesen, J. E. (2023). Challenges in upscaling
641 laboratory studies to ecosystems in soil microbiology research. Global Change Biology, 29(3),
642 569-574. https://doi.org/10.1111/gcb.16537

643 Chevallereau, A., Pons, B. J., van Houte, S., & Westra, E. R. (2022). Interactions between bacterial
644 and phage communities in natural environments. Nature Reviews Microbiology, 20(1), 49-62.
645 https://doi.org/10.1038/s41579-021-00602-y

646 Cortés-Martín, A., Buttimer ,Colin, Maier ,Jessie L., Tobin ,Ciara A., Draper ,Lorraine A., Ross
647 ,R. Paul, Kleiner ,Manuel, Hill ,Colin, & and Shkoporov, A. N. (2025). Adaptations in gut
648 Bacteroidales facilitate stable co-existence with their lytic bacteriophages. Gut Microbes, 17(1),
649 2507775. https://doi.org/10.1080/19490976.2025.2507775

650 Darling, A., Mau, B., Blattner, F., & Perna, N. (2004). Mauve: Multiple Alignment of Conserved
651 Genomic Sequence With Rearrangements. https://genome.cshlp.org/content/14/7/1394

652 De Sordi, L., Khanna, V., & Debarbieux, L. (2017). The Gut Microbiota Facilitates Drifts in the
653 Genetic Diversity and Infectivity of Bacterial Viruses. Cell Host & Microbe, 22(6), 801-808.e3.
654 https://doi.org/10.1016/j.chom.2017.10.010

655 Di Meglio, L., Santos, F., Gomariz, M., Almansa, C., López, C., Antón, J., & Nercessian, D.
656 (2016). Seasonal dynamics of extremely halophilic microbial communities in three Argentinian
657 salterns. FEMS Microbiology Ecology, 92(12), fiw184. https://doi.org/10.1093/femsec/fiw184

658 Duffy, S. (2018). Why are RNA virus mutation rates so damn high? PLOS Biology, 16(8),
659 e3000003. https://doi.org/10.1371/journal.pbio.3000003

660 Fierer, N. (2017). Embracing the unknown: Disentangling the complexities of the soil microbiome.
661 Nature Reviews Microbiology, 15(10), 579-590. https://doi.org/10.1038/nrmicro.2017.87

662 Fuhrman, J. A., Cram, J. A., & Needham, D. M. (2015). Marine microbial community dynamics
663 and their ecological interpretation. Nature Reviews Microbiology, 13(3), 133-146.
664 https://doi.org/10.1038/nrmicro3417

665 Giraud, A., Matic, I., Tenaillon, O., Clara, A., Radman, M., Fons, M., & Taddei, F. (2001). Costs
666 and Benefits of High Mutation Rates: Adaptive Evolution of Bacteria in the Mouse Gut. Science,
667 291(5513), 2606-2608. https://doi.org/10.1126/science.1056421

668 Gomariz, M., Martínez-García, M., Santos, F., Rodriguez, F., Capella-Gutiérrez, S., Gabaldón, T.,
669 Rosselló-Móra, R., Meseguer, I., & Antón, J. (2015). From community approaches to single-cell
670 genomics: The discovery of ubiquitous hyperhalophilic Bacteroidetes generalists. The ISME
671 Journal, 9(1), Article 1. https://doi.org/10.1038/ismej.2014.95

672 Gómez, P., & Buckling, A. (2011). Bacteria-Phage Antagonistic Coevolution in Soil. Science,
673 332(6025), 106-109. https://doi.org/10.1126/science.1198767

674 Gómez, P., & Buckling, A. (2013). Coevolution with phages does not influence the evolution of
675 bacterial mutation rates in soil. The ISME Journal, 7(11), 2242-2244.
676 https://doi.org/10.1038/ismej.2013.105

677 Hernandez, C. A., Delesalle, V. A., Krukonis, G. P., DeCurzio, J. M., & Koskella, B. (2024).
678 Genomic and phenotypic signatures of bacteriophage coevolution with the phytopathogen
679 *Pseudomonas syringae*. Molecular Ecology, 33(10), e16850. https://doi.org/10.1111/mec.16850

680 Holtzman, T., Globus, R., Molshanski-Mor, S., Ben-Shem, A., Yosef, I., & Qimron, U. (2020). A
681 continuous evolution system for contracting the host range of bacteriophage T7. Scientific Reports,
682 10(1), 307. https://doi.org/10.1038/s41598-019-57221-0

683 Jessup, C. M., Kassen, R., Forde, S. E., Kerr, B., Buckling, A., Rainey, P. B., & Bohannan, B. J.
684 M. (2004). Big questions, small worlds: Microbial model systems in ecology. Trends in Ecology
685 & Evolution, 19(4), 189-197. https://doi.org/10.1016/j.tree.2004.01.008

686 Jiang, C., Hwang, Y. T., Randell, J. C. W., Coen, D. M., & Hwang, C. B. C. (2007). Mutations
687 That Decrease DNA Binding of the Processivity Factor of the Herpes Simplex Virus DNA
688 Polymerase Reduce Viral Yield, Alter the Kinetics of Viral DNA Replication, and Decrease the
689 Fidelity of DNA Replication. Journal of Virology, 81(7), 3495-3502.
690 https://doi.org/10.1128/jvi.02359-06

691 Jiang, C., Komazin-Meredith, G., Tian, W., Coen, D. M., & Hwang, C. B. C. (2009). Mutations
692 That Increase DNA Binding by the Processivity Factor of Herpes Simplex Virus Affect Virus
693 Production and DNA Replication Fidelity. Journal of Virology, 83(15), 7573-7580.
694 https://doi.org/10.1128/jvi.00193-09

Kortright, K. E., Chan, B. K., Evans, B. R., & Turner, P. E. (2022). Arms race and fluctuating selection dynamics in *Pseudomonas aeruginosa* bacteria coevolving with phage OMKO1. Journal of Evolutionary Biology, 35(11), 1475-1487. https://doi.org/10.1111/jeb.14095

Koskella, B., Hernandez, C. A., & Wheatley, R. M. (2022). Understanding the Impacts of Bacteriophage Viruses: From Laboratory Evolution to Natural Ecosystems. Annual Review of Virology, 9(Volume 9, 2022), 57-78. https://doi.org/10.1146/annurev-virology-091919-075914

Levin, S. A. (1998). Ecosystems and the Biosphere as Complex Adaptive Systems. Ecosystems, 1(5), 431-436. https://doi.org/10.1007/s100219900037

Longdon, B., Brockhurst, M. A., Russell, C. A., Welch, J. J., & Jiggins, F. M. (2014). The Evolution and Genetics of Virus Host Shifts. PLOS Pathogens, 10(11), e1004395. https://doi.org/10.1371/journal.ppat.1004395

Lourenço, M., Chaffringeon, L., Lamy-Besnier, Q., Pédron, T., Campagne, P., Eberl, C., Bérard, M., Stecher, B., Debarbieux, L., & De Sordi, L. (2020). The Spatial Heterogeneity of the Gut Limits Predation and Fosters Coexistence of Bacteria and Bacteriophages. Cell Host & Microbe, 28(3), 390-401.e5. https://doi.org/10.1016/j.chom.2020.06.002

Middelboe, M., & Brussaard, C. P. D. (2017). Marine Viruses: Key Players in Marine Ecosystems. Viruses, 9(10), Article 10. https://doi.org/10.3390/v9100302

Middelboe, M., Hagström, A., Blackburn, N., Sinn, B., Fischer, U., Borch, N. H., Pinhassi, J., Simu, K., & Lorenz, M. G. (2001). Effects of Bacteriophages on the Population Dynamics of Four Strains of Pelagic Marine Bacteria. Microbial Ecology, 42(3), 395-406. https://doi.org/10.1007/s00248-001-0012-1

Mora-Ruiz, M. del R., Cifuentes, A., Font-Verdera, F., Pérez-Fernández, C., Farias, M. E., González, B., Orfila, A., & Rosselló-Móra, R. (2018). Biogeographical patterns of bacterial and archaeal communities from distant hypersaline environments. Systematic and Applied Microbiology, 41(2), 139-150. https://doi.org/10.1016/j.syapm.2017.10.006

720 Mumford, R., & Friman, V.-P. (2017). Bacterial competition and quorum-sensing signalling shape
721 the eco-evolutionary outcomes of model in vitro phage therapy. Evolutionary Applications, 10(2),
722 161-169. https://doi.org/10.1111/eva.12435

723 Oren, A. (2011). Ecology of Halophiles. En K. Horikoshi (Ed.), Extremophiles Handbook (pp.
724 343-361). Springer Japan. https://doi.org/10.1007/978-4-431-53898-1_16

725 Penchuk, Y., Savytska, M., Kobyliak, N., Ostapchenko, D., Kolodiy, I., Onysenko, S., Tsyryuk,
726 O., Korotkyi, O., Grygoriev, F., & Falalyeyeva, T. (2023). Antimicrobial activity of dietary
727 supplements based on bacterial lysate of *Lactobacillus rhamnosus* DV. Frontiers in Cellular and
728 Infection Microbiology, 13. https://doi.org/10.3389/fcimb.2023.1211952

729 Ramos-Barbero, M. D., Aldeguer-Riquelme, B., Viver, T., Villamor, J., Carrillo-Bautista, M.,
730 López-Pascual, C., Konstantinidis, K. T., Martínez-García, M., Santos, F., Rossello-Mora, R., &
731 Antón, J. (2024). Experimental evolution at ecological scales allows linking of viral genotypes to
732 specific host strains. The ISME Journal, wrae208. https://doi.org/10.1093/ismejo/wrae208

733 Roberts, A. E. L., Kragh, K. N., Bjarnsholt, T., & Diggle, S. P. (2015). The Limitations of In Vitro
734 Experimentation in Understanding Biofilms and Chronic Infection. Journal of Molecular Biology,
735 427(23), 3646-3661. https://doi.org/10.1016/j.jmb.2015.09.002

736 Rodriguez-R, L. M., & Konstantinidis, K. T. (2016). The enveomics collection: A toolbox for
737 specialized analyses of microbial genomes and metagenomes (No. e1900v1). PeerJ Inc.
738 https://doi.org/10.7287/peerj.preprints.1900v1

739 Rodriguez-Valera, F., Ventosa, A., Juez, G., & Imhoff, J. F. (1985). Variation of Environmental
740 Features and Microbial Populations with Salt Concentrations in a Multi-Pond Saltern. Microbial
741 Ecology, 11(2), 107-115. https://doi.org/10.1007/BF02010483

742 Rohwer, F., & Thurber, R. V. (2009). Viruses manipulate the marine environment. Nature,
743 459(7244), 207-212. https://doi.org/10.1038/nature08060

744 Sanchez-Martinez, R., Arani, A., Krupovic, M., Weitz, J. S., Santos, F., & Antón, J. (2025).
745 Episomal virus maintenance enables bacterial population recovery from infection and promotes

746 virus–bacterial coexistence. The ISME Journal, 19(1), wraf066.
747 https://doi.org/10.1093/ismejo/wraf066

748 Sant, D. G., Woods, L. C., Barr, J. J., & McDonald, M. J. (2021). Host diversity slows
749 bacteriophage adaptation by selecting generalists over specialists. Nature Ecology & Evolution,
750 5(3), Article 3. https://doi.org/10.1038/s41559-020-01364-1

751 Santos, F., Yarza, P., Parro, V., Meseguer, I., Rosselló-Móra, R., & Antón, J. (2012). Culture-
752 Independent Approaches for Studying Viruses from Hypersaline Environments. Applied and
753 Environmental Microbiology, 78(6), 1635-1643. https://doi.org/10.1128/AEM.07175-11

754 Shiklomanov, I. A. (1998). World freshwater resources. UNESCO International Hydrological
755 Programme, UNESCO-IHP.

756 Smakman, F., & Hall, A. R. (2022). Exposure to lysed bacteria can promote or inhibit growth of
757 neighboring live bacteria depending on local abiotic conditions. FEMS Microbiology Ecology,
758 98(2), fiac011. https://doi.org/10.1093/femsec/fiac011

759 Subramanian, S., Dover, J. A., Parent, K. N., & Doore, S. M. (2022). Host Range Expansion of
760 *Shigella* Phage Sf6 Evolves through Point Mutations in the Tailspike. Journal of Virology, 96(16),
761 e00929-22. https://doi.org/10.1128/jvi.00929-22

762 Svet, L., Parijs, I., Isphording, S., Lories, B., Marchal, K., & Steenackers, H. P. (2023).
763 Competitive interactions facilitate resistance development against antimicrobials. Applied and
764 Environmental Microbiology, 89(10), e01155-23. https://doi.org/10.1128/aem.01155-23

765 Trejo-Hernández, A., Andrade-Domínguez, A., Hernández, M., & Encarnación, S. (2014).
766 Interspecies competition triggers virulence and mutability in *Candida albicans–Pseudomonas*
767 *aeruginosa* mixed biofilms. The ISME Journal, 8(10), 1974-1988.
768 https://doi.org/10.1038/ismej.2014.53

769 Turner, P. E. (2005). Parasitism Between Co-Infecting Bacteriophages. En R. A. Desharnais (Ed.),
770 Advances in Ecological Research (Vol. 37, pp. 309-332). Academic Press.
771 https://doi.org/10.1016/S0065-2504(04)37010-8

Ventosa, A. (2006). Unusual micro-organisms from unusual habitats: Hypersaline environments. En H. M. Lappin-Scott, N. A. Logan, & P. C. F. Oyston (Eds.), Prokaryotic Diversity: Mechanisms and Significance (pp. 223-254). Cambridge University Press. https://doi.org/10.1017/CBO9780511754913.015

Ventosa, A., de la Haba, R. R., Sánchez-Porro, C., & Papke, R. T. (2015). Microbial diversity of hypersaline environments: A metagenomic approach. Current Opinion in Microbiology, 25, 80-87. https://doi.org/10.1016/j.mib.2015.05.002

Villamor, J., Ramos-Barbero, M. D., González-Torres, P., Gabaldón, T., Rosselló-Móra, R., Meseguer, I., Martínez-García, M., Santos, F., & Antón, J. (2018). Characterization of ecologically diverse viruses infecting co-occurring strains of cosmopolitan hyperhalophilic Bacteroidetes. The ISME Journal, 12(2), Article 2. https://doi.org/10.1038/ismej.2017.175

Viver, T., Cifuentes, A., Díaz, S., Rodríguez-Valdecantos, G., González, B., Antón, J., & Rosselló-Móra, R. (2015). Diversity of extremely halophilic cultivable prokaryotes in Mediterranean, Atlantic and Pacific solar salterns: Evidence that unexplored sites constitute sources of cultivable novelty. Systematic and Applied Microbiology, 38(4), 266-275. https://doi.org/10.1016/j.syapm.2015.02.002

Viver, T., Conrad, R. E., Lucio, M., Harir, M., Urdiain, M., Gago, J. F., Suárez-Suárez, A., Bustos-Caparros, E., Sanchez-Martinez, R., Mayol, E., Fassetta, F., Pang, J., Mădălin Gridan, I., Venter, S., Santos, F., Baxter, B., Llames, M. E., Cristea, A., Banciu, H. L., … Rossello-Mora, R. (2023). Description of two cultivated and two uncultivated new *Salinibacter* species, one named following the rules of the bacteriological code: *Salinibacter grassmerensis* sp. nov.; and three named following the rules of the SeqCode: *Salinibacter pepae* sp. nov., *Salinibacter abyssi* sp. nov., and *Salinibacter pampae* sp. nov. Systematic and Applied Microbiology, 46(3), 126416. https://doi.org/10.1016/j.syapm.2023.126416

Wielgoss, S., Bergmiller, T., Bischofberger, A. M., & Hall, A. R. (2016). Adaptation to Parasites and Costs of Parasite Resistance in Mutator and Nonmutator Bacteria. Molecular Biology and Evolution, 33(3), 770-782. https://doi.org/10.1093/molbev/msv270

Zimmer, C., & Dorea, C. C. (2023). Differences in laboratory versus field treatment performance of point-of-use drinking water treatment methods: Research gaps and ways forward. Npj Clean Water, 6(1), 1-7. https://doi.org/10.1038/s41545-023-00241-1

ACKNOWLEDGEMENTS

We warmly thank the Molecular Microbial Ecology group for their valuable feedback and constructive criticism throughout this work. We also acknowledge the Genomics and Proteomics Unit of the University of Alicante for their assistance with flow cytometry. Special thanks to Antonio Sanchez-Amat and Maliheh Mehrshad for their insightful feedback and suggestions. We thank Beatriz Cámara for developing the script used in the ANIr analysis and Heather Maughan for the professional English editing and critical reading of the manuscript. This research was supported by the projects "VIRHOST" CIPROM/2021/006 (PROMETEO 2022, Generalitat Valenciana) to J.A., and METACIRCLE PID2021-126114NB-C41 to F.S. and J.A. (Spanish Ministry of Science and Innovation). R.S.M. received funding for his doctoral thesis from the Spanish Ministry of Science and Innovation PRE2019-087998. R.S.M., E.R.P., F.S. and J.A. are members of the National Excellence Network FAGOMA (RED2022-134837-T).

AUTHOR CONTRIBUTIONS

F.S. and J.A. conceived the study. R.S.M., F.S., and J.A. designed the experimental approach. R.S.M. performed the experiments and analyzed the sequences under the inputs and supervision of F.S. and J.A. E.R.P. designed the primers and probes for each strain and virus. L.M.R., J.S. and M.E. provided advice and carried out the microfluidics-based qPCR. R.S.M. drafted the original manuscript. All authors contributed to manuscript final writing and approved the final paper.

DATA AVAILABILITY

The raw sequences used were deposited in the NCBI database with BioProject ID PRJNA1294611.

ETHICS DECLARATIONS

The authors declare no competing interests.

845 **FIGURES**

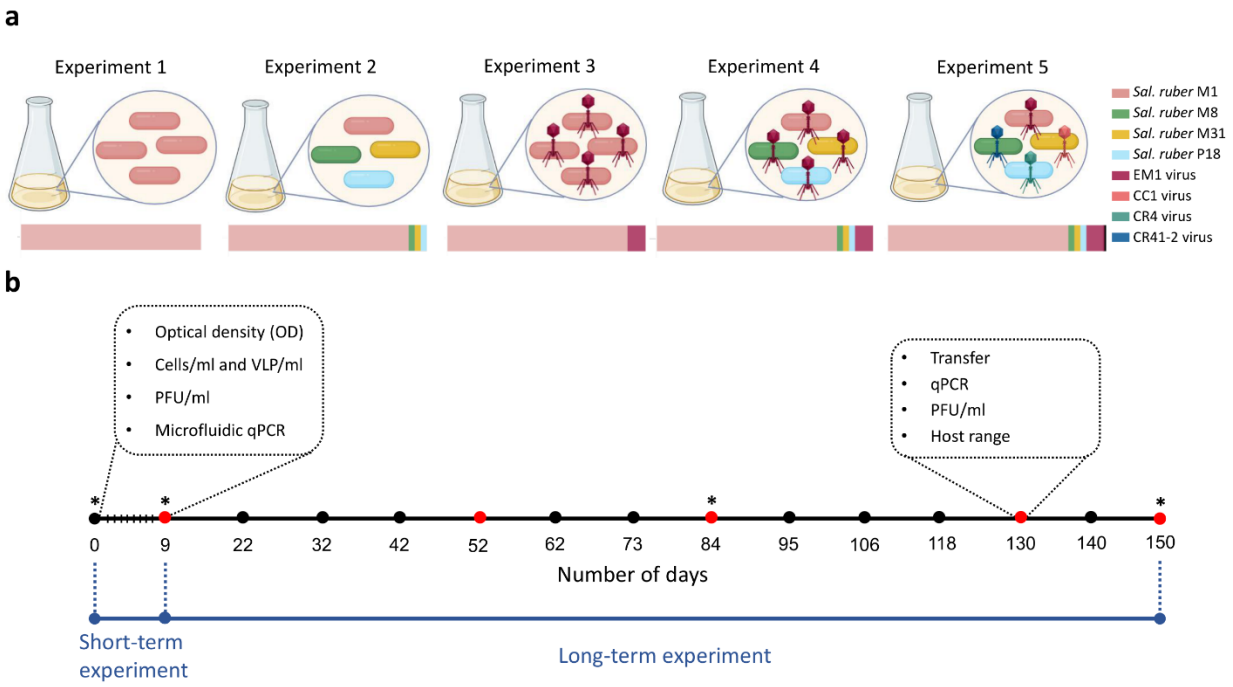

846

847 **Fig. 1**: **Experimental design. a)** Five experiments were conducted using *Sal. ruber* strain M1,
848 with experiments 2, 4, and 5 also inoculated with M8, M31 and P18 strains. Experiments 3, 4, and
849 5 included the EM1 virus, which specifically infects the M1 strain. In experiment 5, the CC1 and
850 CR41-2 viruses, which infect the M8 and M31 strains, and the CR4 virus, which infects the M8
851 strain, were also added. The color bars indicate the proportion of each strain (i.e. cells/ml) or virus
852 (VLP/ml) in the respective experiments. All experiments were performed in triplicate. **b)** In the
853 short-term experiment, samples were incubated for 9 days with regular monitoring. In the long-
854 term experiment, samples were transferred to fresh media every 9-13 days over a 150-day period
855 (black and red dots), with additional parameters measured only at specific points (red dots).
856 Extracellular viromes from experiments 3, 4, and 5 were sequenced at 9, 84, and 150 days, as well
857 as the original viruses (asterisks denote the points chosen for sequencing). Figure created with
858 Biorender.

859

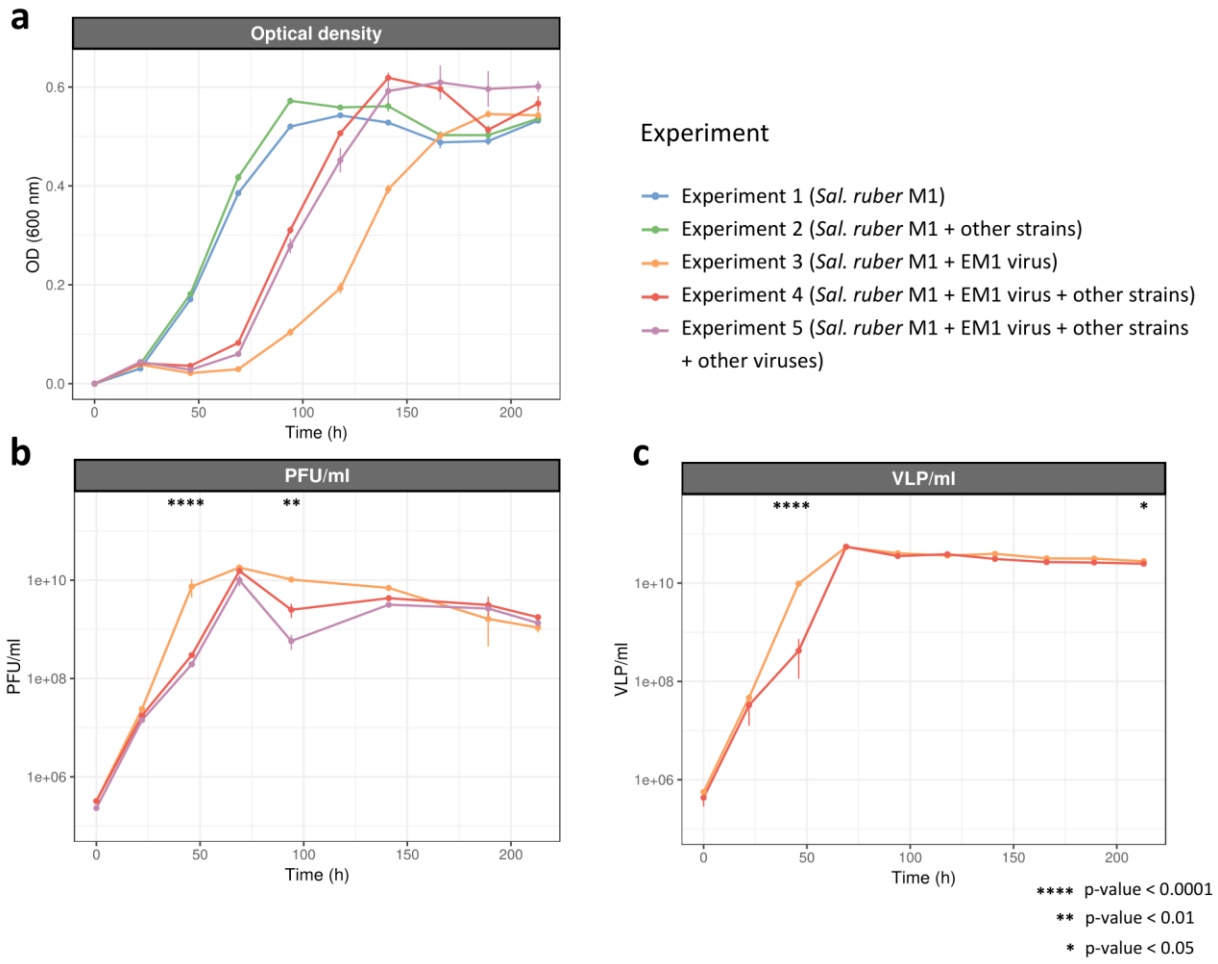

Fig. 2: **Influence of the biological context on the virus-host dynamics in the *Sal. ruber* M1-EM1 pair. a)** Optical density (OD 600 nm) of all five short-term experiments. **b)** PFU/ml of experiments 3, 4 and 5, measured by plaque assay against the original host *Sal. ruber* M1. **c)** Extracellular VLP/ml of experiments 3 and 4 measured by flow cytometry. All the experiments were performed in triplicate. Error bars represent the standard error of the biological replicates. Asterisks indicate significant differences based on one-way ANOVA comparing experiment 3 with experiments 4 and 5. `Other strains´ refers to M8, M31 and P18 strains and `other viruses´ refers to CC1, CR4, and CR41-2 viruses.

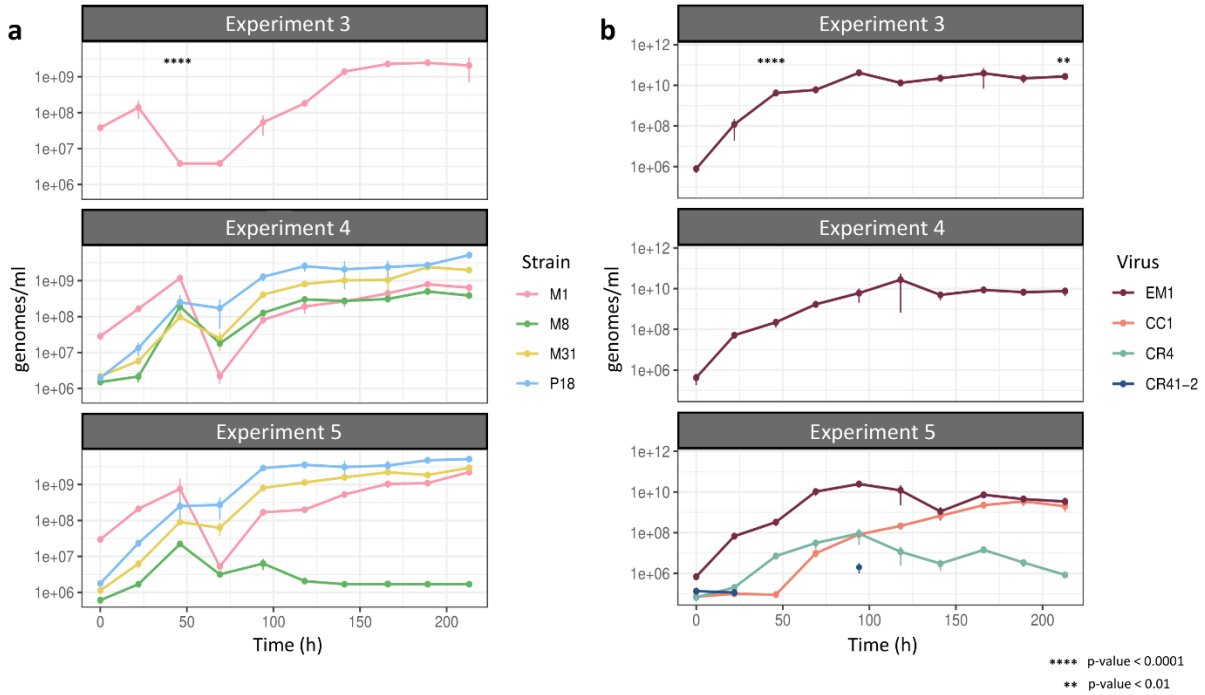

871

872 **Fig. 3**: **Concentration of the different *Sal. ruber* strains and viruses in experiments 3, 4, and**
873 **5. a)** Genomes/ml of each strain in experiments 3, 4 and 5 (top to bottom) measured by microfluidic
874 qPCR. **b**) Free genomes/ml in the supernatant of experiments 3, 4, and 5 (top to bottom) measured
875 by microfluidics-based qPCR. All experiments were performed in triplicate. Error bars represent
876 the standard error of the biological replicates. Asterisks indicate significant differences based on
877 one-way ANOVA comparing experiment 3 with experiments 4 and 5.

878

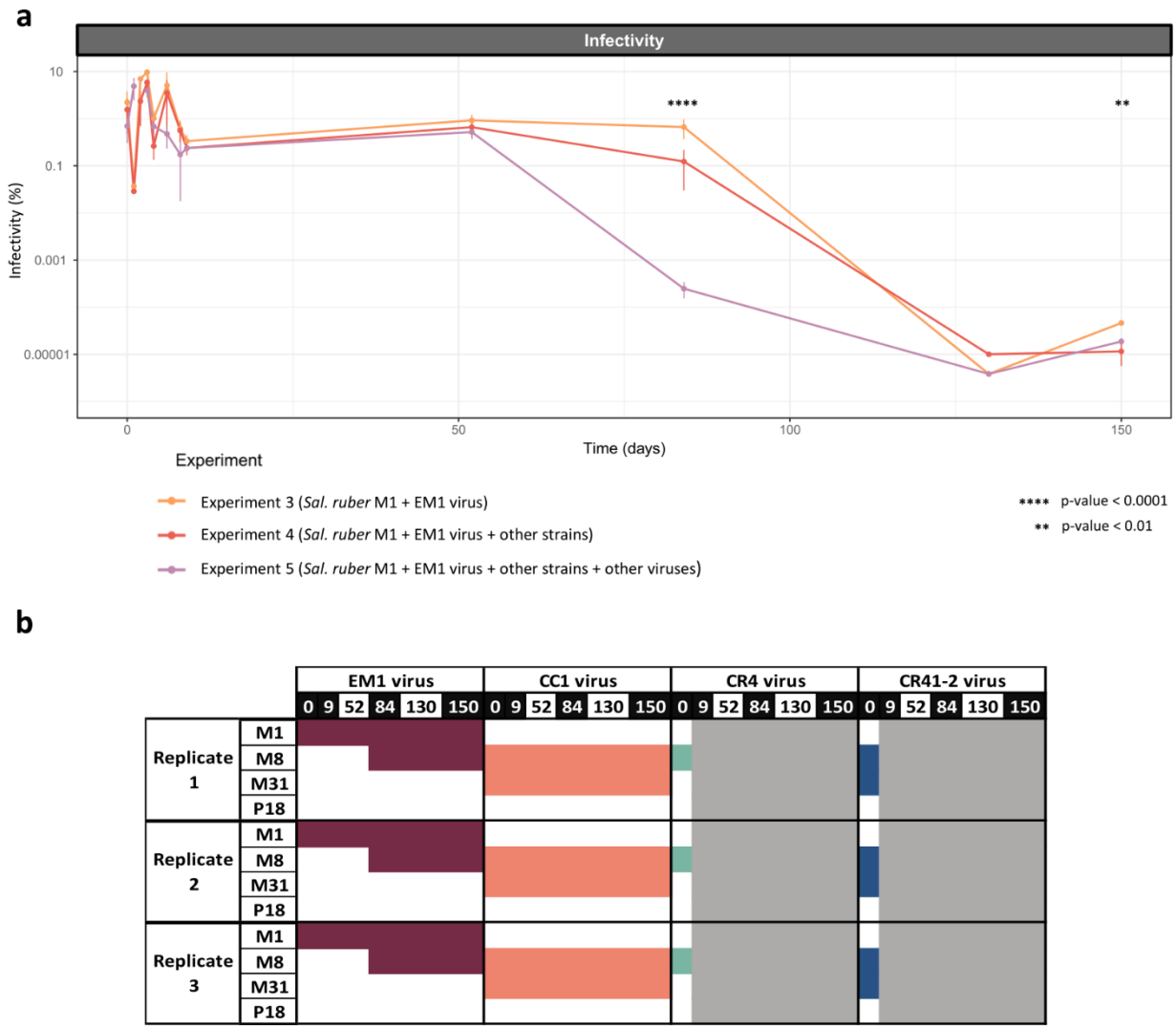

Fig. 4: **The biological context affects the evolution of the infectivity and host range of the EM1 virus. a)** Infectivity of EM1 virus in experiments 3, 4 and 5 in the long-term experiment, defined as the ratio between PFU/ml and extracellular genomes/ml. The y-axis represents the percentage of infectious viruses. Error bars represent the standard error of the biological replicates. Asterisks indicate significant differences based on one-way ANOVA comparing experiment 3 with experiments 4 and 5. **b)** Host range of the four viruses across the three biological replicates in experiment 5. The gray area indicates viral extinction. The time points marked in black (upper part) denote those selected for genomic analysis.

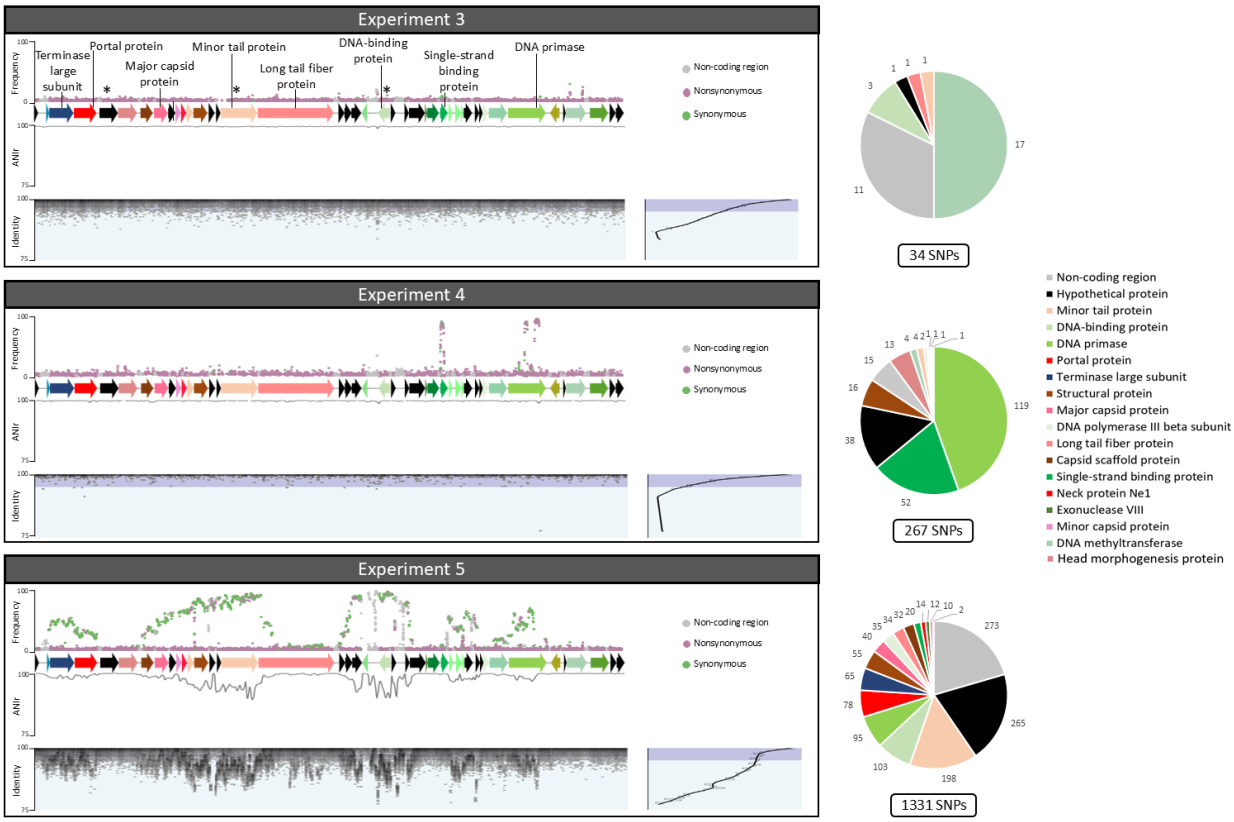

Fig. 5: **Mutations in the EM1 virus genome in the three experiments at 150 days.** The three panels outlined in black represent experiments 3, 4, and 5, from top to bottom. In each panel's upper section, mutations are marked as points across the EM1 genome, with the y-axis indicating mutations frequencies. Below each mutation plot is a representation of the genome of EM1, where arrows represent the open reading frames (ORFs). The middle plot depicts the ANIr along the viral genome, with the y-axis showing the ANIr. In the lower part of each panel, a fragment recruitment plot is shown, where the EM1 genome is positioned at the top as the reference, and gray points represent the reads recruited, with the y-axis showing the percentage of identity for each mapped read. A histogram on the right side of this section indicates the distribution of reads by identity. At the right of the figure, pie charts illustrate the protein-coding genes mutated in each experiment and the number of mutations in each ORF. Proteins selected for metabarcoding are marked with asterisks at the top of the first panel.

903 **EXTENDED DATA**

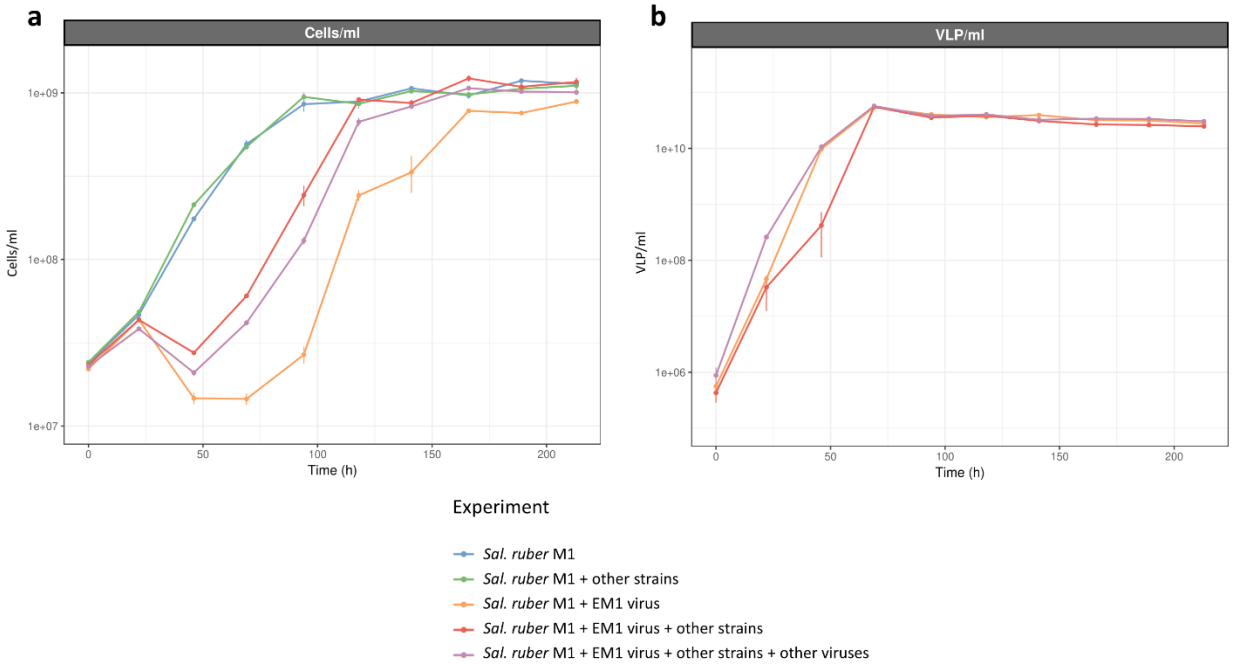

904

905 **Extended Data Fig. 1**: **Cells/ml and VLP/ml measured with flow cytometry. a)** Cells/ml of the
906 five experiments measured using flow cytometry. **b)** VLP/ml of the experiments 3, 4 and 5
907 measured using flow cytometry. All experiments were performed in triplicate. Error bars represent
908 the standard error of the biological replicates.

909

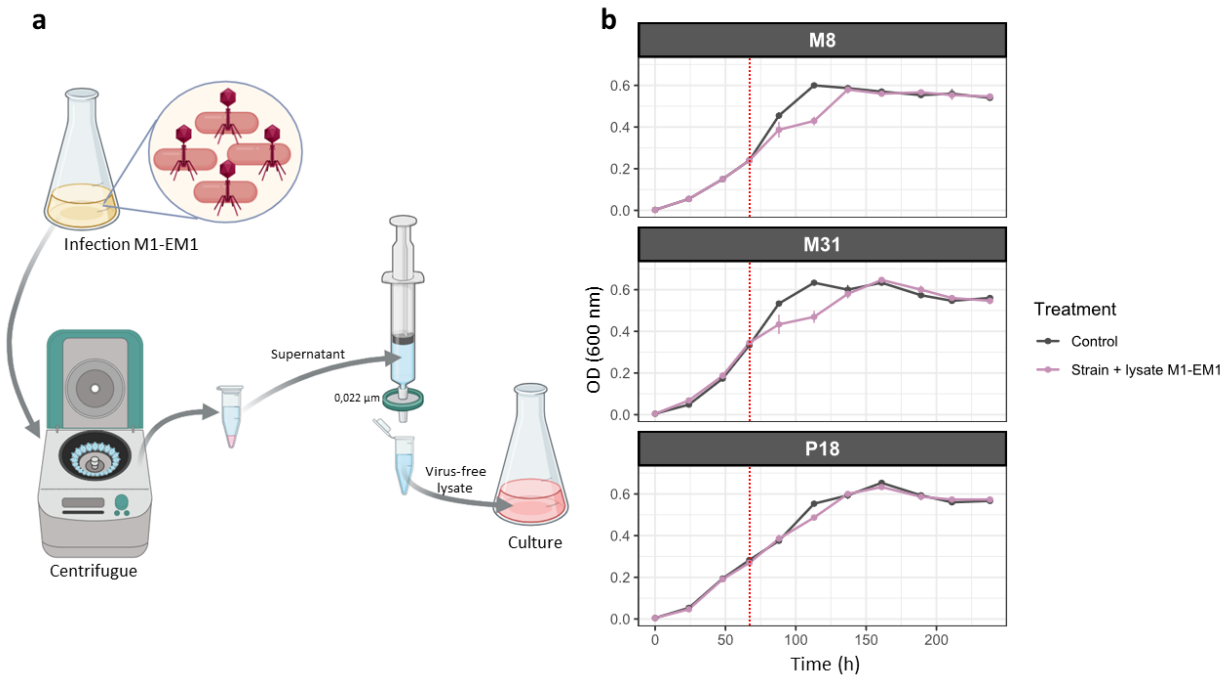

910

911 **Extended Data Fig. 2**: ***Sal. ruber* strains M8, M31 and P18 were exposed to virus-free lysate**
912 **of *Sal. ruber* M1-EM1. a)** The *Sal. ruber* M1-EM1 virus-free lysate was obtained by
913 centrifugation and filtration of the *Sal. ruber* M1-EM1 culture supernatant through a 0.022 µm
914 filter. The lysate was added at 67 hours (red dotted line) to exponential phase cultures of M8, M31
915 and P18 strains. **b)** Growth curves of M8, M31 and P18 amended with lysate (grey) and their
916 corresponding unamended controls (purple). All experiments were performed in triplicate. Error
917 bars represent the standard error of the biological replicates. Figure created with Biorender.

918

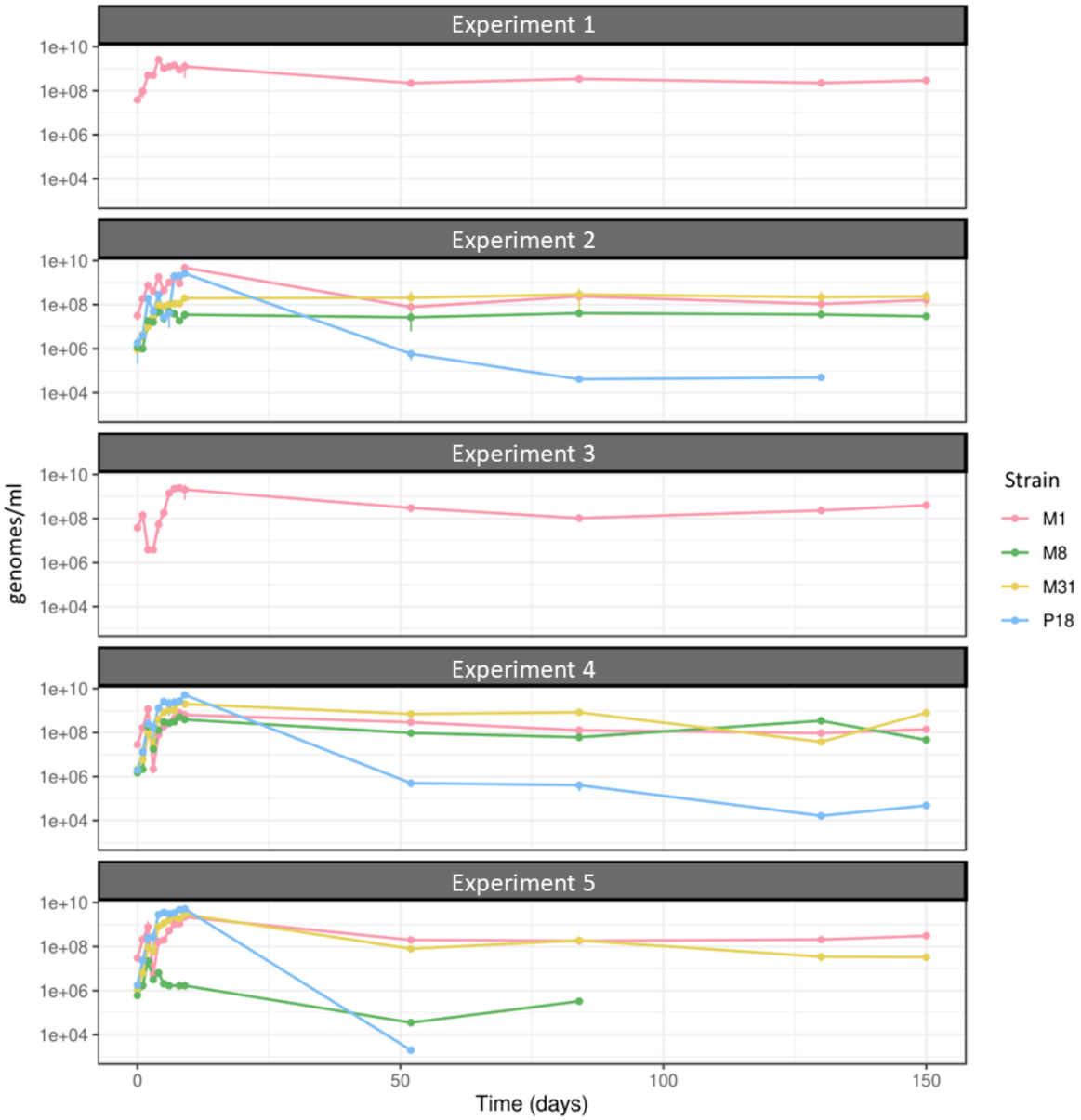

Extended Data Fig. 3: **Concentration of the different *Sal. ruber* strains in the long-term experiment.** Genomes/ml of each strain in the long-term in experiments 1, 2, 3, 4 and 5 (top to bottom) measured by qPCR. All experiments were performed in triplicate. Error bars represent the standard error of the biological replicates.

926

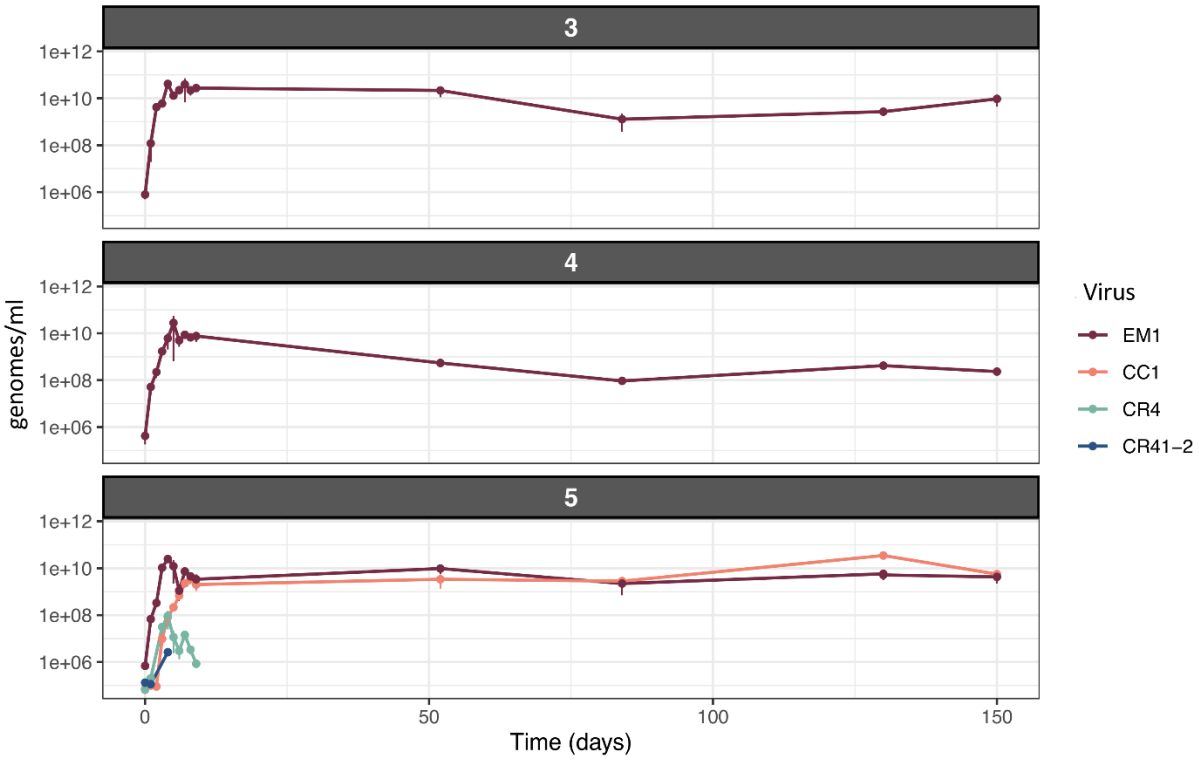

927

928 **Extended Data Fig. 4**: **Concentration of the different extracellular *Sal. ruber* viruses in the**
929 **long-term experiment.** Genomes/ml of each virus in the long-term in experiments 3, 4 and 5 (top
930 to bottom) measured by qPCR. All experiments were performed in triplicate. Error bars represent
931 the standard error of the biological replicates.

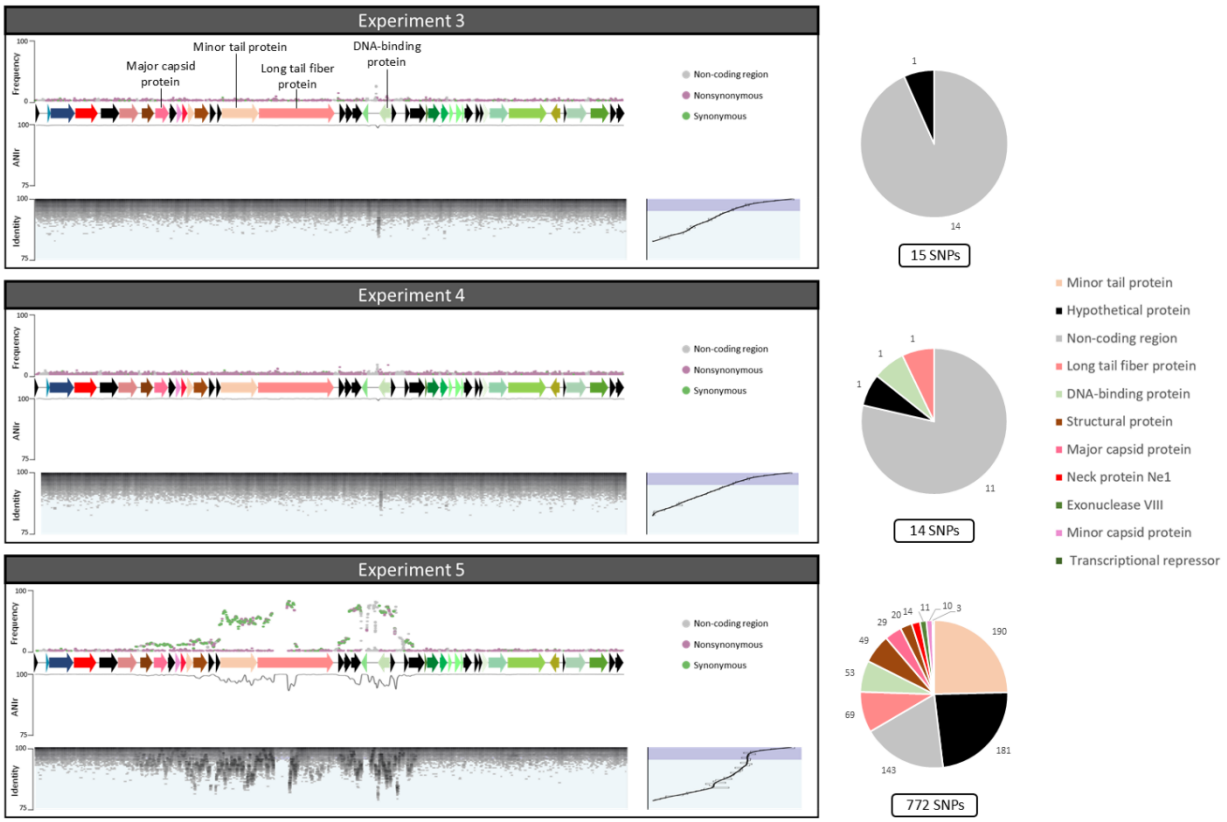

Extended Data Fig. 5: **Mutations in EM1 virus genome in the three experiments at 84 days.** The three panels outlined in black represent experiments 3, 4, and 5, from top to bottom. In each panel's upper section, mutations are marked as points across the EM1 genome, with the y-axis indicating mutation frequencies. Just below each mutation plot there is a representation of the genome of EM1, where arrows represent the open reading frames (ORFs). The middle plot depicts the ANIr along the viral genome, with the y-axis showing the ANIr. In the lower part of each panel, a fragment recruitment plot is shown, where the EM1 genome is positioned at the top as the reference, and gray points represent the reads recruited, with the y-axis showing the percentage of identity for each mapped read. A histogram on the right side of this section indicates the distribution of reads by identity. At the right of the figure, pie charts illustrate the mutated protein-coding genes identified in each experiment and the number of mutations in each ORF.

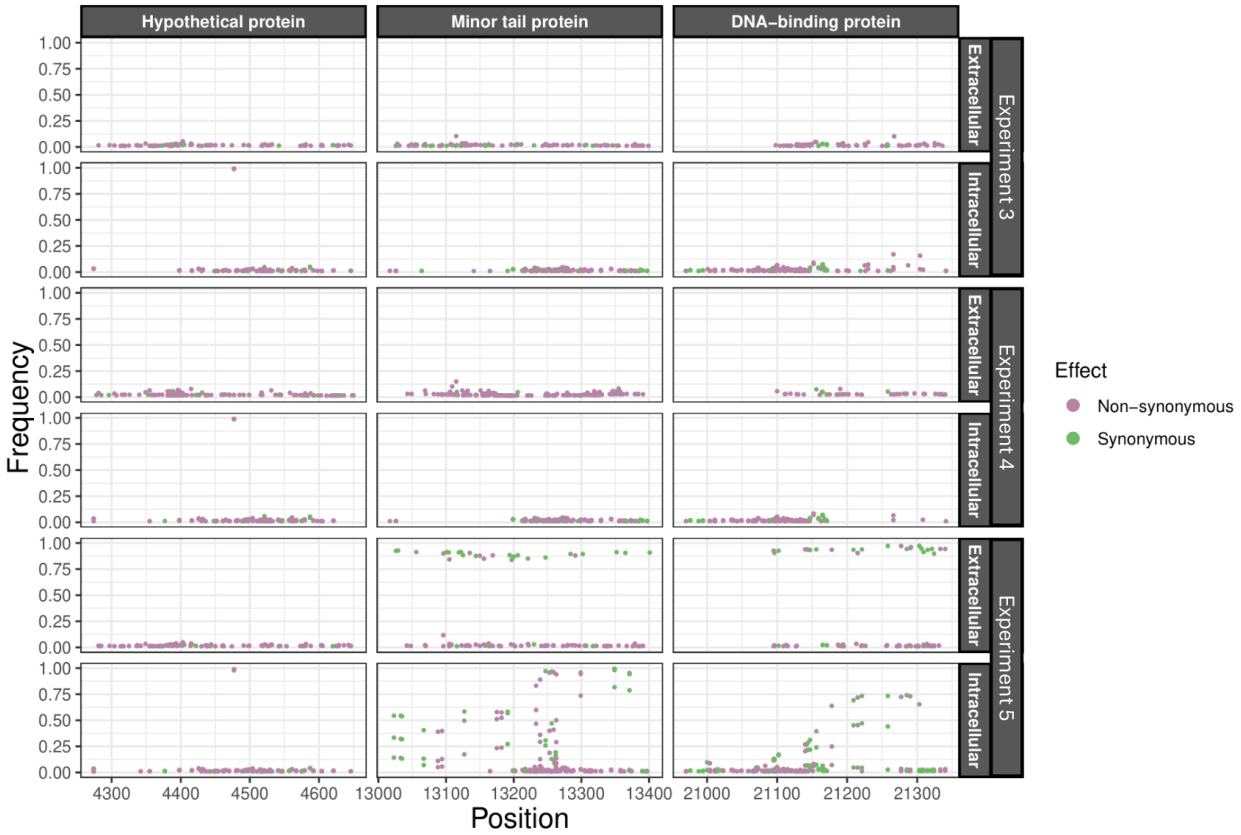

Extended Data Fig. 6: Mutations in the extracellular and intracellular EM1 virus genome across the three proteins selected for metabarcoding. Each column represents one of the three selected proteins. Rows correspond to extracellular and intracellular mutations from experiments 3, 4, and 5 (top to bottom). Mutations are shown as dots along the EM1 genome, with their frequencies indicated on the y-axis.

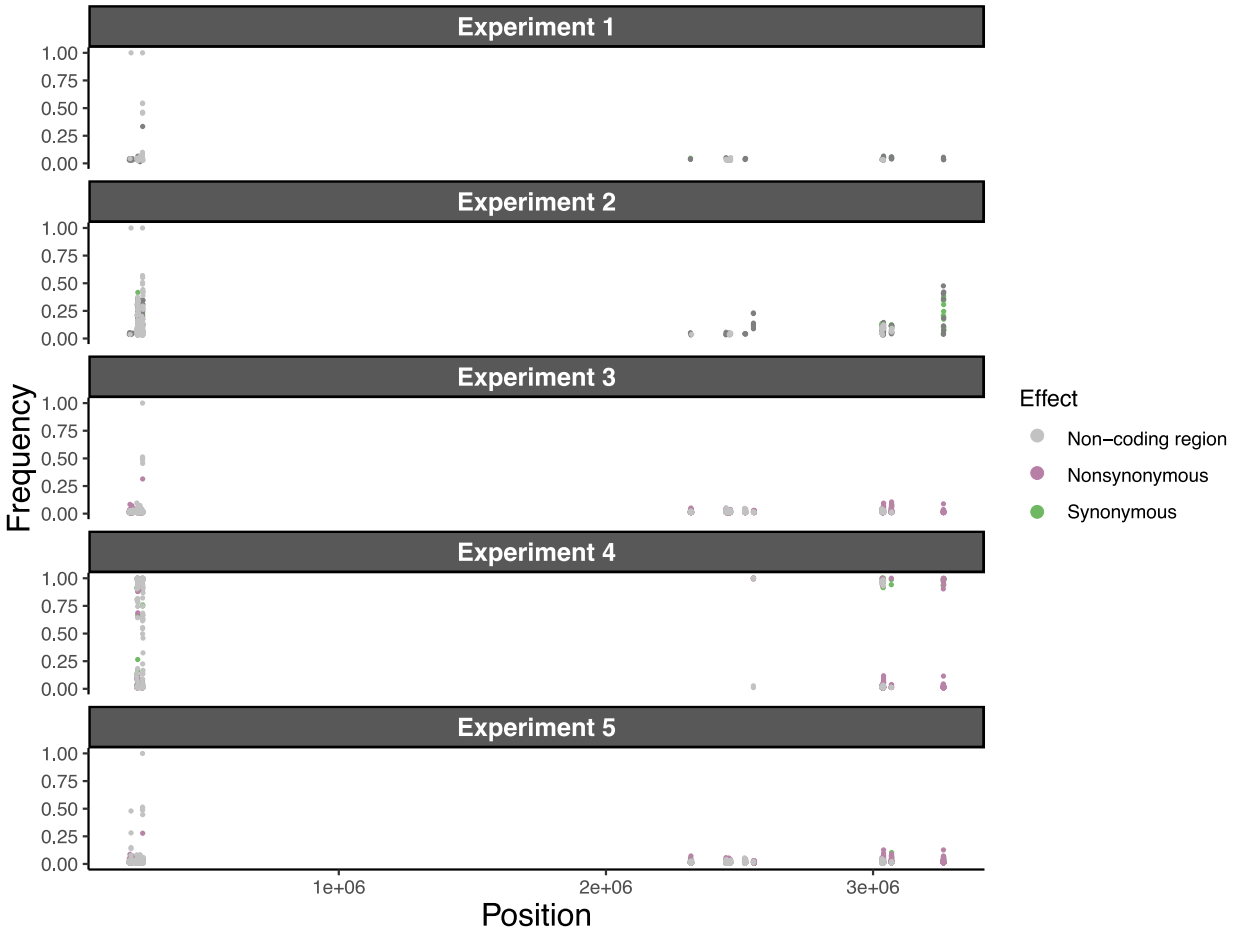

Extended Data Fig. 7: Mutations accumulated in the nine selected regions of the chromosome of *Sal. ruber* M1 at 150 days. The different panels represent experiments 1, 2, 3, 4, and 5, from top to bottom. Mutations are marked as points across the *Sal. ruber* M1 chromosome, with the y-axis indicating mutation frequencies.